Glass-transition asymptotics in two theories of glassy dynamics: Self-consistent generalized Langevin equation and mode-coupling theory

L. F. Elizondo-Aguilera [1] and Th. Voigtmann [1,2]

[1] *Institut für Materialphysik im Weltraum, Deutsches Zentrum für Luft- und Raumfahrt (DLR), 51170 Köln, Germany*

[2] *Department of Physics, Heinrich-Heine-Universität Düsseldorf, Universitätsstraße 1, 40225 Düsseldorf, Germany*

(Received 27 June 2019; published 3 October 2019)

We contrast the generic features of structural relaxation close to the idealized glass transition that are predicted by the self-consistent generalized Langevin equation theory (SCGLE) against those that are predicted by the mode-coupling theory of the glass transition (MCT). We present an asymptotic solution close to conditions of kinetic arrest that is valid for both theories, despite the different starting points that are adopted in deriving them. This in particular provides the same level of understanding of the asymptotic dynamics in the SCGLE as was previously done only for MCT. We discuss similarities and different predictions of the two theories for kinetic arrest in standard glass-forming models, as exemplified through the hard-sphere system. Qualitative differences are found for models where a decoupling of relaxation modes is predicted, such as the generalized Gaussian core model, or binary hard-sphere mixtures of particles with very disparate sizes. These differences, which arise in the distinct treatment of the memory kernels associated to self- and collective motion of particles, lead to distinct scenarios that are predicted by each theory for partially arrested states and in the vicinity of higher-order glass-transition singularities.

DOI: 10.1103/PhysRevE.100.042601

I. INTRODUCTION

The amorphous solidification of an undercooled or compressed liquid into a glassy state is an ubiquitous process in nature and materials physics. The same qualitative features are observed in the slow structural relaxation and in the approach to kinetic arrest in a wide range of microscopically very different materials, be it polymeric and colloidal glasses [1,2], gels [3,4], various metallic alloys [5,6], or bio-inspired models and biological tissue [7–10]. It is a challenging and ferociously debated question, how such generic dynamical features arise from quite different underlying microscopic mechanisms.

Two "first-principles" theories of kinetic arrest—in the sense that they start from the equations of motion of the individual particles in the many-body system—are the mode-coupling theory of the glass transition (MCT) [11–14] and the self-consistent generalized Langevin equation formalism (SCGLE) [15–18]. Both emphasize the role of temporal memory effects in the structural relaxation as described in terms of dynamical density correlation functions, for which both arrive at superficially similar evolution equations. Indeed, both theories give a similarly convincing and often also quantitatively correct account of the slow dynamics as one approaches kinetic arrest. Both take as input parameters information on the microscopic structure of the system (in the form of static structure factors). Yet, the foundations and arguments used to derive MCT and SCGLE differ substantially, and thus it remains unclear whether the numerical similarities between these two approaches are coincidence or specific to certain model systems, or whether they express slightly differing descriptions of the same physical laws. Such questions can only be addressed by a more rigorous mathematical analysis of the respective theories [19].

A qualitative understanding of why kinetic-arrest features are generic requires to explain in which sense the structural-relaxation dynamics (that according to MCT and SCGLE *a priori* depends on the details of the microscopic system) can be understood in terms of "universal" relaxation laws decorated with system-specific prefactors. For MCT, this is achieved by an asymptotic analysis [20,21] that identifies the closeness of structural relaxation to the frozen-in glassy structure as a small parameter σ, and two timescales that diverge as $|\sigma|$ becomes small and thus allow to abstract from the system-specific details of short-time motion. Out of this asymptotic analysis, a number of remarkable statements of MCT follow: for example, that structural relaxation is independent on whether the system's short-time motion is ballistic or diffusive (as verified in computer simulation [22,23]), or that equilibrium structural relaxation is at most diffusive but never superdiffusive or ballistic, i.e., follows stretched but never compressed exponentials [24,25] (as checked against experiment [26]). Such statements depend on the mathematical structure of the MCT equations and on MCT-specific features of the coupling coefficients that are *a priori* different in the SCGLE theory. Importantly, both theories treat the interplay between self- and collective density fluctuations very differently. This becomes relevant in glass formers where these two quantities show a strong decoupling in their long-time relaxation close the glass transition, such as in partially arrested binary mixtures of size-disparate colloids [27,28] or in fast-ion conducting sodium-silicate melts [29,30]. Thus it is an open question in how far SCGLE predicts the same generic features as MCT for the glass transition and where the theories will qualitatively differ.

In this contribution, we address this question by performing an asymptotic analysis of both MCT and SCGLE on an

equal footing. The calculation is based on the recognition that the evolution equations of both theories can be recast in a more general common form, so that the similarities and differences between the two theories can be clearly pinpointed. The technique used in the expansion then is a straightforward generalization of that performed earlier for MCT [20]. This fills a gap in the development of SCGLE, by providing the first asymptotic expansion of this theory close to the glass transition, and by allowing to identify the power laws that describe the divergence of relaxation times within SCGLE in a fashion similar to what is known from MCT.

We show that for "typical" models of glass formers, such as the hard-sphere fluid, the predictions of both MCT and SCGLE are essentially "the same" (in a sense that can be defined by the asymptotic analysis) and point out the significant differences that arise regarding the hydrodynamic limit. We also show that much more interesting (and quite intriguing) differences arise in other models where a decoupling of relaxation modes is found, such as the generalized Gaussian model or, most notably, binary mixtures of large and small particles with a sufficiently large size disparity. In the latter case, both theories agree in predicting both fully arrested glassy states (called the "double glass") as well as partially arrested "single glass" states [27,28]. In the latter, the long-range motion of the large species is suppressed while the small-particle dynamics still shows long-time diffusion. However, the details of the transitions and the structural features of the partially arrested glasses differ qualitatively, and this may in principle be tested in experiments or simulations.

Our work is organized as follows: in Sec. II we briefly review and summarize both SCGLE and MCT, and in Sec. III an asymptotic expansion applicable to both theoretical approaches is carried out. Section IV exhibits specific results for one-component model systems, including the hard-sphere fluid and the generalized Gaussian core model. In Sec. V we turn to a description of the asymptotic kinetic arrest in highly asymmetric binary mixtures of hard spheres as predicted by the two theories. In Sec. VI our concluding remarks are presented.

II. THEORY

We focus here on colloidal glass formers, i.e., systems where the dynamics is posited to follow from the overdamped Langevin equation of motion. This allows a more stringent comparison between MCT and SCGLE, as the latter was originally formulated under this assumption. Within both theories and from simulation, it is well understood that Newtonian systems follow the same long-time behavior [31,32].

Consider a M-component N-particle system of spherical particles in a volume V that are fully characterized by their positions in space, $\vec{r}_j$, $j = 1, \ldots, N$. We denote by N_α the number of particles of a given species; $\sum_\alpha N_\alpha = N$. The number density $n = N/V$, and the partial number densities are given by $n_\alpha = N_\alpha/V$. The quantities $x_\alpha = N_\alpha/N = n_\alpha/n$ are the number concentrations of the individual species, satisfying $\sum_\alpha x_\alpha = 1$.

The fundamental quantity in both SCGLE and MCT is the number-density fluctuation to wave vector $\vec{q}$ of particle species α, $\delta n_\alpha(\vec{q}) = \sum_{j=1}^{N_\alpha} \exp[i\vec{q}\cdot\vec{r}_j^{(\alpha)}]/\sqrt{N_\alpha}$, where the sum is restricted to particles of that species. [A more conventional definition of $\delta n_\alpha(\vec{q})$ is to normalize by $\sqrt{N}$, which differs from ours by a factor $\sqrt{x_\alpha}$.] The time evolution of $\delta n_\alpha(\vec{q})$ is governed by the underlying dynamics of the particles and shall be denoted by $\delta n_\alpha(\vec{q}, t)$. Statistical information on the collective dynamics of these density fluctuations is provided by the dynamical density-correlation functions, also called the matrix of partial intermediate scattering functions (ISFs), $\Phi_{\alpha\beta}(q, t) = \langle \delta n_\alpha^*(\vec{q}, t)\delta n_\beta(\vec{q})\rangle$, where angular brackets indicate the equilibrium ensemble average. We assume that the system remains homogeneous and isotropic throughout, so that $\Phi_{\alpha\beta}(q, t)$ depends on the wave vector only through its modulus $q = |\vec{q}|$. The initial value $\Phi_{\alpha\beta}(q, 0) = S_{\alpha\beta}(q)$ is the matrix of partial static structure factors that characterizes the equilibrium structure of the fluid. Note that $S_{\alpha\beta}(q) \to \delta_{\alpha\beta}$ for $q \to \infty$ in our convention. In both SCGLE and MCT, the static structure functions are assumed to be known quantities from liquid-state theory, and usually one also assumes that they change only regularly over the interesting range of control parameters; by this assumption, thermodynamic phase transitions and critical points are disregarded in order to focus on the kinetic slowing down of the fluidlike amorphous structure.

Structural relaxation in a fluid causes the $\Phi_{\alpha\beta}(q, t)$ to relax from their initial value to zero in a finite time interval. If, however, $\Phi_{\alpha\beta}(q, t)$ does not decay fully over a given time interval, the system reacts as a nonergodic solid with respect to density fluctuations of that species and wave number within the corresponding time window: some finite overlap between initial and final particle configurations remains on average, indicative of solidlike behavior. Thus, a quantity of central interest is the long-time limit

$$F_{\alpha\beta}(q) = \lim_{t\to\infty} \Phi_{\alpha\beta}(q, t). \tag{1}$$

States where $F_{\alpha\beta}(q) \neq 0$ are identified as idealized glasses, and the points where the long-time limit $F_{\alpha\beta}(q)$ changes from zero to a nonzero value are identified as ideal fluid-glass transitions. The quantities $F_{\alpha\beta}(q)$ are commonly referred to as the nonergodicity parameters (NEP) of the system, the glass form factors, or sometimes the Debye-Waller factors.

The tagged-particle density correlation functions or self-intermediate scattering functions (sISFs) are given by $\Phi_\alpha^s(q, t) = \langle \delta n_\alpha^{s*}(\vec{q}, t)\delta n_\alpha^s(\vec{q})\rangle$, where $\delta n_\alpha^s(\vec{q}) = \exp[i\vec{q}\cdot\vec{r}_s^{(\alpha)}]$ is the tagged-particle density fluctuation for a particle labeled s of species α. One has $\Phi_\alpha^s(q, 0) = 1$ for the initial value. The sISFs quantify the statistics of the individual movements of particles in the system. They are often denoted as $\Phi_\alpha^s(q, t) = \langle \exp[i\vec{q}\cdot\Delta\vec{r}^{(\alpha)}(t)]\rangle$, where $\Delta\vec{r}^{(\alpha)}(t)$ is the time-dependent displacement of any of the particles of species α. The sISF is related to the mean-squared displacement $\delta r_\alpha^2(t) = \langle \Delta\vec{r}^{(\alpha)}(t)^2\rangle$ through its $q \to 0$ limit.

If long-range particle motion ceases, $\delta r_\alpha^2(t)$ remains bounded, and $\Phi_\alpha^s(q, t)$ does not relax to zero for long times. Hence, the long-time limit $F_\alpha^s(q) = \lim_{t\to\infty} \Phi_\alpha^s(q, t)$ allows us to distinguish states where particles of species α are delocalized [$F_\alpha^s(q) = 0$] from those where they are localized [$F_\alpha^s(q) > 0$]. The points where $F_\alpha^s(q)$ first becomes nonzero can thus be identified as idealized single-particle arrest

transitions. The quantity $F_\alpha^s(q)$ is referred to as the tagged-particle NEP or Lamb-Mößbauer factor.

For notational convenience, we will denote matrices in the species indices by bold symbols and introduce a label $\varsigma \in \{, s\}$ to distinguish collective from tagged-particle quantities. Writing $\Phi^s_{\alpha\beta}(q,t) = \delta_{\alpha\beta}\Phi^s_\alpha(q,t)$, we will thus denote by $\boldsymbol{\Phi}^\varsigma(q,t)$ the collection of both ISFs and sISFs of the system. Its initial values are denoted by $\boldsymbol{S}(q)$ and $\boldsymbol{S}^s(q) = \mathbf{1}$, respectively. The $\boldsymbol{\Phi}^\varsigma(q,t)$ form a matrix algebra if matrix multiplication with respect to the species indices is understood in the usual sense for any fixed q and fixed ς. A scalar product on this matrix algebra shall be defined by $(\boldsymbol{A},\boldsymbol{B}) := \sum_\varsigma \sum_q \boldsymbol{A}^\varsigma(q){:}\boldsymbol{B}^\varsigma(q)$, where: denotes the double contraction over the species indices. For mathematical caution, we will assume all wave-number indices q to come from a countable range (as is initially the case before performing the thermodynamic limit); however, the usual replacement $(1/V)\sum_{\vec{q}} \mapsto 1/(2\pi)^d \int d^d q$ shall be made in writing the SCGLE and MCT equations. We exclusively deal with three-dimensional, $d = 3$, systems for simplicity. Neither from MCT nor from SCGLE does one expect a crucial qualitative change in asymptotic behavior with (finite) dimensionality.

For certain purposes, it is convenient to introduce the *propagators* $\boldsymbol{\Psi}(q,t) = \boldsymbol{\Phi}(q,t)\cdot\boldsymbol{S}^{-1}(q)$ and $\boldsymbol{\Psi}^s(q,t) = \boldsymbol{\Phi}^s(q,t)$ [18,28]. They obey $\boldsymbol{\Psi}^\varsigma(q,0) = \mathbf{1}$. However, care has to be taken: the features of the equilibrium overdamped Langevin dynamics ensure that $\boldsymbol{\Phi}^\varsigma(q,t)$ are symmetric positive definite matrices at all times [25]; this property is lost for $\boldsymbol{\Psi}^\varsigma(q,t)$.

Evolution equations for $\boldsymbol{\Phi}^\varsigma(q,t)$ can be obtained in various ways. The central notion is that, although the statistical-mechanics evolution of the system is a Markov process, the evolution of the restricted set of dynamical variables $\delta n^\varsigma_\alpha(\vec{q})$ is non-Markovian. Either starting from a generalized Langevin equation [15,17] in the first place or by a formal manipulation of the initial Markov dynamics using Mori-Zwanzig projection operators [11,33], one obtains

$$\boldsymbol{L}^\varsigma(q)\cdot\dot{\boldsymbol{\Phi}}^\varsigma(q,t) + (\boldsymbol{S}^\varsigma)^{-1}\cdot\boldsymbol{\Phi}^\varsigma(q,t) + \int_0^t \boldsymbol{m}^\varsigma(q,t-t')\cdot\dot{\boldsymbol{\Phi}}^\varsigma(q,t')\,dt' = \mathbf{0}, \tag{2}$$

where the overdot indicates differentiation with respect to time and $L^\varsigma_{\alpha\beta}(q) = \delta_{\alpha\beta}/q^2 D^0_\alpha$ sets the short-time relaxation through the particles' short-time diffusivities D^0_α. (Hydrodynamic interactions in a suspending fluid are ignored here.) The memory kernel $\boldsymbol{m}^\varsigma(q,t)$ represents retarded friction effects and is essential to capture the non-Markovian relaxation of density fluctuations. It is, in the context of Brownian dynamics, referred to as the irreducible memory kernel and is the central object to be approximated in both SCGLE or MCT.

In the remainder of this section, we summarize the approximations of both SCGLE and MCT; we refer to the original literature for details of the derivation [11,16]. In essence, SCGLE starts from the point of view of single-particle arrest causing a decrease in mobility that in turn mediates the collective relaxation; MCT on the other hand emphasizes the collective effects of particle motion and treats the single-particle mobility as a mere consequence of such collective effects. Hence, the role played by $\Phi^s_\alpha(q,t)$ is quite different in the two theories.

A. SCGLE

The SCGLE is based on the generalized Langevin equation formalism [34] and the concept of a contraction of the description from many variables to few [35]. We summarize here the version obtained for a multicomponent colloidal system [17,18].

One starts from the assumption that the glass transition is governed by local fluctuations and that in the relevant range of finite q, the collective friction can be expressed in some form of superposition of single-particle friction contributions. Thus the memory functions $\boldsymbol{m}(q,t)$ and $\boldsymbol{m}^s(q,t)$ should be closely related at finite q. It has been found [15,17] that the simplest of these relations, referred to as the *zero-order* Vineyard-like approximation, is sufficient to obtain a good description of the long-time dynamics, even if this ignores the consequence of translational invariance (momentum conservation in the statistical average) for the collective dynamics. The approximation consists in setting $\boldsymbol{m}^\varsigma(q,t) = \boldsymbol{L}^\varsigma(q)\cdot\boldsymbol{C}^\varsigma(q,t)$ and equating

$$\boldsymbol{C}(q,t) \approx \boldsymbol{C}^s(q,t). \tag{3}$$

In the hydrodynamic limit, $q \to 0$, the memory function $C^s_\alpha(q,t)$ should reduce to a time-dependent friction coefficient $\Delta\zeta^*_\alpha(t)$ that describes the non-Markovian contribution of the direct interactions to the friction coefficient of a tagged particle of species α [36]. For $q \to \infty$, on the other hand, one expects the contributions from $C^s_\alpha(q,t)$ to vanish. One thus further approximates

$$C^s_\alpha(q,t) \approx \lambda_\alpha(q)\Delta\zeta^*_\alpha(t), \tag{4a}$$

where

$$\lambda_\alpha(q) = \left[1 + \left(q/k^c_\alpha\right)^2\right]^{-1} \tag{4b}$$

is an empirical interpolation function characterized by *ad hoc* cutoff wave numbers k^c_α. The latter are sometimes related to the position $k^{\max}_\alpha$ of the maximum of $S_{\alpha\alpha}(q)$ by $k^c_\alpha = a k^{\max}_\alpha$. The single free parameter a is then determined by a calibration procedure such that the predicted glass transition of the theory is in reasonable agreement with, for instance, the one determined from simulations [37]. Generically, increasing the k^c_α will cause increasing contributions to the memory function and hence shift the predicted glass-transition point to lower densities.

The time-dependent friction $\Delta\zeta^*_\alpha(t)$ is obtained from a self-consistent closure of the generalized Langevin equation as [34–36]

$$\Delta\zeta^*_\alpha(t) = \frac{nD^0_\alpha}{24\pi^3}\int d^3k\, k^2 [\boldsymbol{\Psi}^s(k,t)]_{\alpha\alpha} \times [\boldsymbol{h}(k)\cdot\sqrt{\boldsymbol{n}}\cdot\boldsymbol{\Psi}(k,t)\cdot\sqrt{\boldsymbol{n}}\cdot\boldsymbol{h}(k)]_{\alpha\alpha}. \tag{5}$$

Here, $\boldsymbol{n}$ is the diagonal matrix of partial densities, $n_{\alpha\beta} = \delta_{\alpha\beta}n_\alpha$, and $\boldsymbol{h}(q)/n$ is the matrix of static total correlation functions related to the static structure factor by $\boldsymbol{S}(q) = \mathbf{1} + \boldsymbol{h}(q)$. The notation $[\boldsymbol{A}]_{\alpha\beta}$ is used here to refer to the α,β-element of a matrix $\boldsymbol{A}$. For later reference, let us denote the long-time

limit of the friction kernel as

$$\bar{\zeta}_\alpha = \lim_{t\to\infty} \Delta\zeta^*_\alpha(t)/D^0_\alpha. \tag{6}$$

For the present purpose, it is convenient to rewrite Eqs. (3) to (5) in the form

$$m^\varsigma_{\alpha\beta}(q,t) = \delta_{\alpha\beta}\frac{n\lambda_\alpha(q)}{6\pi^2 q^2}\sum_{\alpha'\beta'\alpha''\beta''}\int_0^\infty dk\, k^4 \times \hat{c}^\varsigma_{\alpha\alpha'}(k)\hat{c}^{\bar{\varsigma}}_{\alpha\alpha''}(k)\hat{c}^\varsigma_{\beta\beta'}(k)\hat{c}^{\bar{\varsigma}}_{\beta\beta''}(k)\Phi^\varsigma_{\alpha'\beta'}(k,t)\Phi^{\bar{\varsigma}}_{\alpha''\beta''}(k,t), \tag{7}$$

denoting by $\bar{\varsigma}$ the label opposite to ς. The auxiliary function $\hat{c}^\varsigma_{\alpha\beta}(k)$ is defined in terms of the Ornstein-Zernike direct correlation function $c_{\alpha\beta}(k)$ by $\hat{c}_{\alpha\beta}(k) = c_{\alpha\beta}(k)\sqrt{x_\alpha}$ and $\hat{c}^s_{\alpha\beta}(k) = \delta_{\alpha\beta}$. Recall that the $\boldsymbol{c}(k)$ are related to the static structure factor by $\boldsymbol{S}^{-1}(k) = \mathbf{1} - \sqrt{\boldsymbol{n}}\cdot\boldsymbol{c}(k)\cdot\sqrt{\boldsymbol{n}}$.

Equation (7) emphasizes a number of features of $\boldsymbol{m}^\varsigma(q,t)$: it is a symmetric bilinear form of the $\boldsymbol{\Phi}(k,t)$ and $\boldsymbol{\Phi}^s(k,t)$, with coupling coefficients that depend only on the static structural properties of the system. In particular it does not depend on the kinetic parameters that characterize the short-time motion; i.e., it is independent on D^0_α. Equation (7) together with Eq. (2) provides a closed set of equations to determine simultaneously the collective, $\boldsymbol{\Phi}(q,t)$, and the tagged-particle, $\boldsymbol{\Phi}^s(q,t)$, density correlation functions of the glass-forming mixture.

B. MCT

Following a Zwanzig-Mori projection technique, the irreducible collective friction kernel $\boldsymbol{m}(q,t)$ is a correlation function of fluctuating forces $\delta\vec{f}_\alpha(\vec{q})$ propagated dynamically in the subspace orthogonal to the one-point density fluctuations. MCT proceeds by assuming that the slow dynamics of these forces is dominated by their structural contributions. The approximation thus consists of expressing the fluctuating forces through their overlap with density-pair fluctuations, $\delta n_\beta(\vec{k})\delta n_\gamma(\vec{p})$, with $\vec{k}+\vec{p}=\vec{q}$ in order to satisfy momentum balance in the statistical average. As a result, the memory kernel $\boldsymbol{m}(q,t)$ is approximated through a dynamical four-point density correlation function evolving with the reduced propagator. This in turn is approximated by the product of two-point density correlation functions, at the same time replacing the reduced propagator with the full one. (This splitting is not just a Gaussian approximation—a subtle point that is sometimes overlooked.)

For the case of mixtures, the procedure results in [38]

$$m_{\alpha\beta}(q,t) = \frac{n}{2q^2}\int\frac{d^3k}{(2\pi)^3}\sum_{\alpha'\beta'\alpha''\beta''} V_{\alpha\alpha'\alpha''}(\vec{q},\vec{k},\vec{p}) \times V_{\beta\beta'\beta''}(\vec{q},\vec{k},\vec{p})\Phi_{\alpha'\beta'}(k,t)\Phi_{\alpha''\beta''}(p,t). \tag{8a}$$

The coupling vertices are obtained after an additional approximation of static triplet correlations in terms of two-point quantities as

$$V_{\alpha\alpha'\alpha''}(\vec{q},\vec{k},\vec{p}) = (\vec{q}\cdot\vec{k}/q)\hat{c}_{\alpha\alpha'}(k)\delta_{\alpha\alpha''} + (\vec{q}\cdot\vec{p}/q)\hat{c}_{\alpha\alpha''}(p)\delta_{\alpha\alpha'}. \tag{8b}$$

For the tagged-particle memory kernel, the simplest nontrivial overlap of the fluctuating forces $\delta\vec{f}^s_\alpha(\vec{q})$ with structural quantities is with $\delta n^s_\beta(\vec{k})\delta n_\gamma(\vec{p})$. Repeating the steps to obtain $\boldsymbol{m}(q,t)$ *mutatis mutandi* [or alternatively, considering a $(M+1)$-component mixture in the limit where $x_{M+1}\to 0$], one gets

$$m^s_{\alpha\beta}(q,t) = \delta_{\alpha\beta}\frac{1}{q^2}\int\frac{d^3k}{(2\pi)^3}\sum_{\alpha'\beta'} V^s_{\alpha\alpha'\beta'}(\vec{q},\vec{k}) \times \Phi_{\alpha'\beta'}(k,t)\Phi^s_\alpha(p,t), \tag{9a}$$

with vertices

$$V^s_{\alpha\alpha'\beta'}(\vec{q},\vec{k}) = (\vec{q}\cdot\vec{k}/q)^2\hat{c}_{\alpha\alpha'}(k)\hat{c}_{\alpha\beta'}(k). \tag{9b}$$

As in SCGLE, the memory kernels are found to be independent on kinetic parameters, i.e., on D^0_α. Equations (8) and (9) emphasize that in MCT, $\boldsymbol{m}(q,t)$ is a bilinear functional of the $\boldsymbol{\Phi}(k,t)$, where the tagged-particle dynamics does not enter; the tagged-particle kernel $\boldsymbol{m}^s(q,t)$ is, as in SCGLE, a bilinear functional of $\boldsymbol{\Phi}(k,t)$ and $\boldsymbol{\Phi}^s(p,t)$. Equations (2) and (8) thus form a closed set of equations that determines the collective density correlation functions $\boldsymbol{\Phi}(q,t)$. Once these are known, Eqs. (2) and (9) determine the tagged-particle correlation functions $\boldsymbol{\Phi}^s(q,t)$.

The projection-operator formalism used to derive the MCT equations ensures that the theory recovers the expected conservation laws and symmetries. Technically, it is reflected by the appearance of wave numbers $\vec{k}$ and $\vec{p}=\vec{q}-\vec{k}$ in both memory kernels, while the SCGLE expression of these memory kernels contains only couplings to fluctuations to wave vector $\vec{k}$.

III. ASYMPTOTICAL SOLUTION

Both SCGLE and MCT approximate the memory kernels $\boldsymbol{m}^\varsigma(q,t)$ as a bilinear functional of the $\boldsymbol{\Phi}^\varsigma(k,t)$. The main difference in structure is, first, that, in MCT, the $\varsigma = s$ terms do not enter in the collective memory kernel, and that in SCGLE the wave-vector integral has a simpler structure involving only the wave vector $\vec{k}$ and not $\vec{p}=\vec{q}-\vec{k}$. This structure is reminiscent of the $q\to 0$ limit that is also discussed within MCT [21,39] in the context of generalized hydrodynamics. Note, however, that the differences in the low-q structure of the theories have important consequences for the determination of collective transport coefficients. For example, the generalized elastic moduli of the mixtures are determined by Green-Kubo relations that can, in MCT-like approximations, be related to the combinations $\sum_{\alpha\beta}\sqrt{x_\alpha}m_{\alpha\beta}(q,t)\sqrt{x_\beta}$ in the limit $q\to 0$. Although all nontrivial individual elements of $m_{\alpha\beta}(q,t)$ diverge as $\sim 1/q^2$ in that limit (for both MCT and SCGLE), this particular combination remains finite in MCT, while it does not generically do so within SCGLE. A similar difference arises in the determination of the interdiffusion coefficient; we discuss this briefly in Sec. VI.

Despite these differences, both theories share the same mathematical structure,

$$\boldsymbol{m}^\varsigma(t) = \mathcal{F}[\boldsymbol{\Phi}^{\varsigma'}(t), \boldsymbol{\Phi}^{\varsigma''}(t)] \tag{10a}$$

or more specifically

$$m^{\varsigma}_{\alpha\beta}(q,t) = \sum_{\alpha'\beta'\alpha''\beta''\varsigma'\varsigma''} \sum_{\vec{k}\vec{p}} V^{\varsigma\varsigma'\varsigma''}_{\alpha\alpha'\alpha''}(\vec{q},\vec{k},\vec{p}) \times V^{\varsigma\varsigma'\varsigma''}_{\beta\beta'\beta''}(\vec{q},\vec{k},\vec{p})\Phi^{\varsigma'}_{\alpha'\beta'}(k,t)\Phi^{\varsigma''}_{\alpha''\beta''}(p,t), \quad (10b)$$

where the vertices can be read off by comparison with Eq. (7) [augmented with $[(1-\delta_{\varsigma'\varsigma''})/2]^2$], respectively, with Eqs. (8) and (9).

Equation (10) represents a common structure: the memory kernel is a tensor product of the $\mathbf{\Phi}$, contracted with a vertex vector V both from the left and from the right. (This property is typically lost in nonequilibrium extensions of MCT.) As a result, the functional $\mathcal{F}$ preserves positive definiteness: if the matrices $\mathbf{\Phi}(t)$ are positive definite (in the sense defined by our matrix algebra, i.e., for every wave number and every ς), so will be $\boldsymbol{m}(t)$. This in turn ensures that the solutions $\mathbf{\Phi}(t)$ of the evolution equation (2) closed with either SCGLE or MCT will preserve an exact property dictated by the Brownian dynamics: they will be completely monotone functions, i.e., they can be written as the superposition of purely relaxing exponentials whose weights are positive definite matrices. This was known for the MCT solutions [25] and is hereby extended to those of SCGLE. As a consequence, both theories preserve exactly the feature that equilibrium structural relaxation in a Brownian system is never of compressed-exponential or superdiffusive form.

We are interested in the long-time behavior of the solutions of Eq. (2) with Eq. (10). Let us thus assume that $t \gg t_0$, where t_0 is some timescale associated to the decay of density fluctuations without memory effects. Retaining only those terms that will contribute to kinetic arrest at long times, we replace Eq. (2) by an equation of structural relaxation [40]

$$\mathbf{0} = \boldsymbol{S}\cdot\boldsymbol{m}(t)\cdot\boldsymbol{S} - \mathbf{\Phi}(t) - \boldsymbol{S}\cdot\frac{d}{dt}\int_0^t \boldsymbol{m}(t-t')\cdot\mathbf{\Phi}(t')\,dt', \quad (11)$$

which amounts to dropping the term containing only the time derivative of the correlation function in the original evolution equation, and where the q and ς dependence is understood implicitly.

In Eq. (11), the kinetic parameters D^0_α that characterize the short-time motion of the system have dropped out. A similar conclusion holds for the masses in a system undergoing Newtonian dynamics, under the mild assumption that the system is not completely underdamped at large times. Thus, Eq. (11) predicts that the dynamics close to the ideal glass transition is asymptotically independent on kinetic parameters such as the ratios of free-particle mobilities or mass ratios. Recent molecular-dynamics and Brownian-dynamics simulations strongly support this prediction [41].

Anticipate that close to the glass transition, the solutions $\mathbf{\Phi}(t)$ of either theory describe a two-step structural relaxation: there emerges an increasingly large intermediate-time window over which $\mathbf{\Phi}(t) \approx \boldsymbol{F}^c$, where $\boldsymbol{F}^c$ is the long-time limit of the correlation function at the transition. An asymptotic solution to Eq. (11) shall be constructed in the time window where $|\mathbf{\Phi}(t) - \boldsymbol{F}^c|$ is small. This occurs for $t/t_0 \gg 1$ on some timescale t_σ. Writing $\hat{t} = t/t_\sigma$, we start with the ansatz

$$\mathbf{\Phi}(\hat{t}t_\sigma) = \boldsymbol{F}^c + \sqrt{|\sigma|}\boldsymbol{G}^{(1)}(\hat{t}) + |\sigma|\boldsymbol{G}^{(2)}(\hat{t}) + O(|\sigma|^{3/2}). \quad (12)$$

The timescale t_σ will later be fixed such that the expansion terms in Eq. (12) remain of the required order in $|\sigma|$ for long times.

A. Nonergodicity parameters

To order $O(\sigma^0)$, inserting Eq. (12) into Eq. (11) gives the equation relating the critical nonergodicity parameter $\boldsymbol{F}^c$ to the memory kernel evaluated at the transition point. Rearranging terms, one gets

$$(\boldsymbol{S}^c - \boldsymbol{F}^c)^{-1} = (\boldsymbol{S}^c)^{-1} + \boldsymbol{m}^c[\boldsymbol{F}^c, \boldsymbol{F}^c]. \quad (13)$$

Here and in the following, the superscript c marks quantities that are evaluated at the glass-transition point. In fact, Eq. (13) holds for the long-time limit $\boldsymbol{F} = \lim_{t\to\infty}\mathbf{\Phi}(t)$ also off the critical point when dropping the superscripts c.

Equation (13) is a nonlinear implicit equation for $\boldsymbol{F}^c$ and may as such have many different solutions. Based on the fact that the memory kernel preserves positive definiteness, one shows that the long-time limit of the correlation function $\mathbf{\Phi}^c(t)$ is the largest positive (semidefinite) solution of Eq. (13) [25]. As a consequence, a simple iterative scheme to solve Eq. (13) (taking $\boldsymbol{S}^c$ as the initial guess for $\boldsymbol{F}^c$) is guaranteed to converge to the desired solution. Further, Eq. (13) contains possible bifurcation points, where depending on the control parameters entering $\boldsymbol{m}$, new branches of positive definite solutions appear. These bifurcation points are the glass-transition points of MCT or SCGLE. Note that $\boldsymbol{F} = \mathbf{0}$ (corresponding to the fluid state) is always a solution and for sufficiently small coupling coefficients will be the physical one. Equation (13) then allows for fluid-glass transitions; it also, depending on the model system, allows for glass-glass transitions that mark the discontinuous change from one ideal glass to another one with differing mechanical properties, and are signaled by jumps in $\boldsymbol{F}$ from one positive-definite value to another.

Inserting the SCGLE form of the memory kernel in Eq. (13), one arrives at (now dropping c superscripts)

$$\boldsymbol{F}_{\mathrm{SCGLE}}(q) = \boldsymbol{S}(q)\cdot\left[\boldsymbol{S}(q) + \frac{q^2}{\boldsymbol{\lambda}(q)\bar{\boldsymbol{\zeta}}}\mathbf{1}\right]^{-1}\cdot\boldsymbol{S}(q), \quad (14)$$

where $\mathbf{1}/\boldsymbol{\lambda}(q)\bar{\boldsymbol{\zeta}}$ is to be read as $\delta_{\alpha\beta}/\lambda_\alpha(q)\bar{\zeta}_\alpha$. Equation (14) highlights the role played by $\bar{\zeta}_\alpha$ in determining the localization length of the individual species. The expression can be inserted in the definition of the memory kernel to yield a closed nonlinear equation for the $\bar{\zeta}$ which is routinely solved in the framework of SCGLE to determine the glass transition. From Eq. (14) one also readily reads off the $q \to 0$ limit of the SCGLE nonergodicity parameters, $\boldsymbol{F}_{\mathrm{SCGLE}}(q\to 0) \to \boldsymbol{S}(q)$. For the normalized one-component case, this is equivalent to $f(q\to 0) \to 1$. Within MCT, this only holds for the self-part of the dynamics, not the collective part. There, the nonergodic state is characterized by a (mechanical) susceptibility $\tilde{\chi} = (1 - f(0))\chi_T$ that is less than the isothermal susceptibility from the thermodynamic equation of state, χ_T. The SCGLE approximation amounts to stating that the glass is an infinitely rigid solid [42].

Equation (13) can be rewritten as $\boldsymbol{\Psi} = \boldsymbol{F} \cdot \boldsymbol{S}^{-1} = [\boldsymbol{S}^{-1} + \boldsymbol{m}]^{-1} \cdot \boldsymbol{m}$. Within SCGLE, recall that $m^{\sigma}_{\alpha\beta}(q,t) = \delta_{\alpha\beta}(\lambda_\alpha(q)/q^2)\bar{\zeta}_\alpha(t)$. In particular, individual elements of $\bar{\zeta}_\alpha[\boldsymbol{F}]$ can vanish for a subset of the species, say, labeled by $\bar{\alpha}$. In this case, one obtains a "mixed glass" or "partially arrested" state [18] where the corresponding $\Psi_{\alpha\bar{\alpha}} = 0$ although $\boldsymbol{F}$ generically is a fully occupied matrix. In other words, for a mixed glass state, the nonergodicity matrix of the propagator $\boldsymbol{\Psi}$ has zero eigenvalues (one for each mobile species). This is different from the MCT prediction: there, $\boldsymbol{m}$ is a strictly positive definite matrix for all glassy states, including those where the self-dynamics of some species relaxes to zero. But then $\boldsymbol{\Psi}$ is the product of two positive definite matrices and as such has (strictly) positive eigenvalues only; and the same holds for $\boldsymbol{F}$. We shall investigate this issue numerically in Sec. V.

B. Critical amplitudes

To order $O(|\sigma|^{1/2})$, one gets from Eq. (12)

$$\boldsymbol{G}^{(1)}(\hat{t}) + \boldsymbol{S}^c \cdot \boldsymbol{m}^c[\boldsymbol{F}^c, \boldsymbol{F}^c] \cdot \boldsymbol{G}^{(1)}(\hat{t}) = 2\boldsymbol{S}^c \cdot \boldsymbol{m}^c[\boldsymbol{F}^c, \boldsymbol{G}^{(1)}(\hat{t})] \cdot (\boldsymbol{S}^c - \boldsymbol{F}^c). \tag{15}$$

This has to hold for arbitrary $\hat{t}$, and thus the time- and wave-vector dependence of $\boldsymbol{G}^{(1)}(\hat{t})$ split,

$$\boldsymbol{G}^{(1)\varsigma}(q,\hat{t}) = \boldsymbol{H}^{\varsigma}(q) g(\hat{t}). \tag{16}$$

This is known as the factorization theorem within MCT [11]. It implies that, close to the glass-transition point, correlation functions to different wave numbers can be scaled on top of each other by q- and observable-dependent prefactors to show a common, generic time dependence. The scaling function $g(\hat{t})$ will be determined in next order of the σ-expansion. The critical amplitude $\boldsymbol{H}$ satisfies, rearranging terms with the help of Eq. (13),

$$\boldsymbol{H} = 2(\boldsymbol{S}^c - \boldsymbol{F}^c) \cdot \boldsymbol{m}^c[\boldsymbol{F}^c, \boldsymbol{H}] \cdot (\boldsymbol{S}^c - \boldsymbol{F}^c). \tag{17}$$

This is an eigenvalue equation for a linear map on the algebra of (k, ς)-dependent matrices,

$$\boldsymbol{H} = \boldsymbol{C}^c[\boldsymbol{H}]. \tag{18}$$

Equations (13) and (18) jointly determine the glass-transition points: While Eq. (13) holds for the long-time limit generally, the condition that $\boldsymbol{H}$ is an eigenvector of $\boldsymbol{C}^c$ to eigenvalue unity provides the selection criterion for critical points. To this eigenvector there also corresponds a left-eigenvector $\hat{\boldsymbol{H}}$ defined by $(\hat{\boldsymbol{H}}, \boldsymbol{f}) = (\hat{\boldsymbol{H}}, \boldsymbol{C}[\boldsymbol{f}])$ for any trial matrix $\boldsymbol{f}$. We abbreviate the normalization as

$$\mathcal{N} = (\hat{\boldsymbol{H}}, \boldsymbol{H} \cdot (\boldsymbol{S}^c - \boldsymbol{F}^c)^{-1} \cdot \boldsymbol{H}). \tag{19}$$

The properties of $\boldsymbol{C}$ are important in determining the possible asymptotic behavior and are in turn determined by the structure of the coupling vertices. Within MCT, one has that $\boldsymbol{C}$—only for the collective part, $\varsigma = \{\}$—is an irreducible map in the sense of Perron and Frobenius [25]. As such, it is guaranteed to have a nondegenerate maximum eigenvalue which is the spectral radius, with an associated eigenvector that can be chosen strictly positive. One further proves that the spectral radius of $\boldsymbol{C}$ is always bounded by unity. Hence, there is a unique critical amplitude $\boldsymbol{H}$ associated to those control-parameter points where a unit eigenvalue of $\boldsymbol{C}^c$ indeed appears. As a consequence of the fact that the critical eigenvalue of $\boldsymbol{C}^c$ is nondegenerate, the glass-transition singularities in MCT belong to the A_ℓ class of bifurcations in the classification due to Arnol'd [11]. Note that Eq. (18) is equivalent to the statement that the implicit equation (13) can no longer uniquely be inverted locally around $\boldsymbol{F}^c$ because the first-order Taylor expansion term is degenerate; at least two solutions merge in the bifurcation point. In principle, more than two solutions can merge in a single point, and this would be signaled by degeneracies in further Taylor expansion terms. We will in the following consider critical points of the most generic type, i.e., where just two solutions merge (A_2 singularities or standard glass-transition singularities). A consequence is that the generic transition described by MCT for the collective dynamics is *discontinuous*—at the critical point, a nonzero $\boldsymbol{F}^c$ first emerges as the physical solution of Eq. (13), and thus the long-time limit of $\boldsymbol{\Phi}(t)$ jumps from zero to that value.

The fact that within MCT the tagged-particle dynamics ($\varsigma = s$) does not enter this determination of critical points opens the possibility for separate tagged-particle critical points. Because the tagged-particle correlation functions $\boldsymbol{\Phi}^s(t)$ couple only linearly into the respective memory kernel, the generic case here is not a bifurcation of the kind described above, but rather a *continuous* increase of $\boldsymbol{F}^s$ from zero to nonzero values.

In SCGLE, $\boldsymbol{C}$ has a relatively simple structure. Switching to a discrete spectrum of q for simplicity, we obtain

$$H^{\varsigma}_{\alpha\beta}(q) = \sum_{q'\alpha'\beta'\varsigma'} C^{\varsigma\varsigma'}_{q\alpha\beta,q'\alpha'\beta'} H^{\varsigma'}_{\alpha'\beta'}(q') = \sum_{q'\alpha'\beta'\varsigma'} v^{\varsigma}_{q\alpha\beta} \bar{v}^{\varsigma'}_{q'\alpha'\beta'} H^{\varsigma'}_{\alpha'\beta'}(q'). \tag{20}$$

Obviously this implies that $\boldsymbol{H}(q) \propto \boldsymbol{v}_q = [\boldsymbol{S}^c(q) - \boldsymbol{F}^c(q)] \cdot [\boldsymbol{\lambda}(q)/q^2] \cdot [\boldsymbol{S}^c(q) - \boldsymbol{F}^c(q)]$ (where $\boldsymbol{\lambda}$ is the diagonal matrix of the λ_α). Again, $\boldsymbol{C}$ has a nondegenerate eigenvector, and the condition that the corresponding eigenvalue is unity defines the glass-transition point as a bifurcation point in the nonlinear equations. However, in SCGLE this statement includes both the collective and the tagged-particle dynamics simultaneously. Note that even in partially arrested states, all entries of $\boldsymbol{H}(q)$ within SCGLE are nonvanishing, which verifies the applicability of the Perron-Frobenius theorem.

The discussion of the linear map (18) emphasizes a substantial difference between MCT and SCGLE. In the one-component case, the latter theory essentially deals with a single scalar "dynamic order parameter" [see also Eq. (14)] $\gamma = \bar{\zeta}^{-1} = \lim_{t\to\infty} \delta r^2(t)/6$ [18] that is the squared localization length of a particle in the glass. In MCT, at least in principle, the tagged-particle dynamics can remain unarrested in the glass, even for a one-component fluid. We will discuss such a case in Sec. IV. Extending to mixtures, the MCT statement that the collective structure of the glass is qualitatively the same both in the single and the double glass may be an oversimplification that SCGLE addresses differently; we will come back to this point in Sec. V.

C. Scaling function

In order $O(|\sigma|)$, we have to take into account that the coefficients in Eqs. (10) and (11) change when one considers state points slightly off the critical point. Hence,

$$(\mathbf{1}-\boldsymbol{C})[\boldsymbol{G}^{(2)}(\hat{t})] = (\boldsymbol{S}^c-\boldsymbol{F}^c)\cdot\boldsymbol{m}^c[\boldsymbol{H},\boldsymbol{H}]\cdot(\boldsymbol{S}^c-\boldsymbol{F}^c)g(\hat{t})^2 - 2(\boldsymbol{S}^c-\boldsymbol{F}^c)\cdot\boldsymbol{m}^c[\boldsymbol{F}^c,\boldsymbol{H}]\cdot\boldsymbol{H}\partial_{\hat{t}}(g*g)(\hat{t}) + (\boldsymbol{S}^c-\boldsymbol{F}^c)\cdot(\boldsymbol{S}^c)^{-1}\cdot\Delta\boldsymbol{m}/|\sigma|, \tag{21a}$$

where $(f*g)(t)=\int_0^t f(t-t')g(t')\,dt'$ and

$$\Delta\boldsymbol{m}=\boldsymbol{S}\cdot\boldsymbol{m}[\boldsymbol{F}^c,\boldsymbol{F}^c]\cdot(\boldsymbol{S}^c-\boldsymbol{F}^c)-\boldsymbol{S}^c\cdot\boldsymbol{m}^c[\boldsymbol{F}^c,\boldsymbol{F}^c]\cdot(\boldsymbol{S}^c-\boldsymbol{F}^c). \tag{21b}$$

Taking the scalar product with $\hat{\boldsymbol{H}}$ on both sides, the left-hand side vanishes, and there remains

$$0=\lambda g(\hat{t})^2-\frac{d}{d\hat{t}}\int_0^{\hat{t}} g(\hat{t}-\hat{t}')g(\hat{t}')\,d\hat{t}'+\operatorname{sgn}\sigma \tag{22}$$

with the definitions

$$\lambda=(\hat{\boldsymbol{H}},(\boldsymbol{S}^c-\boldsymbol{F}^c)\cdot\boldsymbol{m}^c[\boldsymbol{H},\boldsymbol{H}]\cdot(\boldsymbol{S}^c-\boldsymbol{F}^c))/\mathcal{N} \tag{23}$$

and

$$\sigma=(\hat{\boldsymbol{H}},(\boldsymbol{S}^c-\boldsymbol{F}^c)\cdot(\boldsymbol{S}^c)^{-1}\cdot\Delta\boldsymbol{m})/\mathcal{N} \tag{24}$$

with normalization given by Eq. (19). There holds $\lambda\in[1/2,1]$ for discontinuous transitions [11]. We will assume $\lambda<1$ tacitly in the following; the case $\lambda=1$ corresponds to that of a higher-order singularity. The last equation fixes the expansion parameter σ in terms of control-parameter distances. Consider the case where the transition is driven by a change in a given physical control parameter, say, the density n. The control-parameter distance is usually defined as $\varepsilon=(n-n^c)/n^c$, and it obeys $\varepsilon>0$ in the glass and $\varepsilon<0$ in the liquid. From the definition of $\Delta\boldsymbol{m}$ it is clear, that *asymptotically* close to the transition, there holds $\sigma\propto\varepsilon$, so that both small parameters play the same role.

Equation (22) is the celebrated β-scaling equation of MCT. It holds for SCGLE as well. This transfers a remarkable feature of MCT also to SCGLE: the appearance of nonuniversal power laws (time fractals) with exponents a and b. In particular, Eq. (22) has, for the cases $\lambda<1$, power-law solutions of the form $g(\hat{t})\sim\hat{t}^x$. The time-dependent terms of Eq. (22) balance if the exponent is chosen to obey

$$\lambda=\frac{\Gamma(1-a)^2}{\Gamma(1-2a)}=\frac{\Gamma(1+b)^2}{\Gamma(1+2b)} \tag{25}$$

with $a,b>0$, denoting separately the solutions for $x=-a<0$ and $x=b>0$. Thus, λ is referred to as the exponent parameter of the theory. Since λ is determined by the vertices entering the memory kernel, the power laws $\hat{t}^{-a}$ and $\hat{t}^b$ are generic in the sense that they appear irrespective of the microscopic details of the model under study; but they are nonuniversal in the sense that the numerical values of the exponents depend on these microscopic details.

In detail, at the critical point, $\sigma=0$, the asymptotic solution converges for $\hat{t}\to\infty$ if one sets $g(\hat{t})=\hat{t}^{-a}$. From demanding that the second term in Eq. (12) remains of order unity at $t=t_0$, one fixes $t_\sigma=t_0|\sigma|^{-1/2a}$. This timescale diverges as one approaches the transition, and there opens a window for the so-called critical decay law, identified as the short-time asymptote in the rescaled time of Eq. (22).

For $\sigma\neq0$, the critical decay law is cut off at long times. If $\sigma<0$, Eq. (22) admits the long-time asymptote $g(\hat{t})\sim-B\hat{t}^b$, valid for $t/t_\sigma\gg1$ but $t/t'_\sigma\ll1$, where $t'_\sigma=t_0|\sigma|^{-1/2a-1/2b}$ is fixed by demanding that $|\sigma|^{1/2}\hat{t}^b$ is of order unity at $t=t'_\sigma$. This power law is the so-called von Schweidler law [11], and it describes the decay of the correlation functions from the intermediate-time plateau $\boldsymbol{F}^c$ on the liquid side of the glass transition ($\sigma<0$). The coefficient B of the von Schweidler law depends (only) on λ and is fixed numerically by matching the asymptotic solutions $\hat{t}^{-a}$ and $\hat{t}^b$ of Eq. (22). Note that as $\sigma\to0^-$, both t_σ and t'_σ diverge, but also the ratio t'_σ/t_σ. Thus, an increasingly large time window opens where the relaxation of the correlation function is described by the scaling law. For $\sigma>0$, $g(\hat{t})\to$ const as $\hat{t}\to\infty$ replaces the von Schweidler law and describes arrested solutions in the glass.

In summary, the leading-order asymptotic expansion of the correlation functions in either SCGLE or MCT is, at transition points with $\lambda<1$, using $t=\hat{t}t_\sigma$ and recalling $\boldsymbol{\Phi}(t)=\boldsymbol{F}^c+\sqrt{|\sigma|}\boldsymbol{H}g(\hat{t})$:

$$\boldsymbol{\Phi}(t)=\boldsymbol{F}^c+\boldsymbol{H}(t/t_0)^{-a} \quad \text{for } t\gg t_0, t\ll t_\sigma, \tag{26a}$$

$$\boldsymbol{\Phi}(t)=\boldsymbol{F}^c-\tilde{\boldsymbol{H}}(t/t'_\sigma)^b \quad \text{for } t_\sigma\ll t\ll t'_\sigma, \sigma<0, \tag{26b}$$

$$\boldsymbol{\Phi}(t)=\boldsymbol{F}^c+\hat{\boldsymbol{H}}\sqrt{\sigma} \quad \text{for } t_\sigma\ll t, \sigma>0. \tag{26c}$$

IV. ONE-COMPONENT GLASS TRANSITIONS

We first exemplify the similarities and differences between the theories for simple one-component model systems. For numerical calculations, we discretize wave-number integrals by an equidistant grid of M points, with grid spacing Δq. Unless mentioned otherwise, calculations were performed with $M=400$ and $\Delta q=0.1/R$. The implied large-k cutoff of $Q=40/R$ is reasonably large to not affect the results qualitatively. The grid used here is somewhat finer than the one used by default in many MCT calculations, and somewhat coarser than that used in previous SCGLE calculations.

The nonergodicity parameters $\boldsymbol{F}$ were determined by iteratively solving Eq. (13) for both theories. To determine glass-transition points, a bifurcation search in the control parameters was performed to maximize the largest real eigenvalue e of Eq. (18). While true critical points are characterized by $e=1$, the value of e obtained in the numerical procedure indicates the precision with which parameters like the exponent parameter λ can be given. We typically demand $|e-1|\leqslant10^{-3}$ or better. The equations in the time domain for the full theories were solved by an algorithm outlined in Ref. [26]. We report all dynamical quantities as functions of time t in units of the free-diffusion time $\tau_0=R^2/D^0=1$.

A. Hard-sphere system (HSS)

The prototypical theoretical reference system for the structural glass transition is that of monodisperse hard spheres (HSs) of diameter R. The system has a single control parameter, expressed as a dimensionless packing fraction $\varphi=(\pi/6)nR^3$. We choose the diameter as the unit of length, introducing dimensionless wave numbers $\tilde{q}=qR$. For the static structure factor $S(q)$, the standard Percus-Yevick (PY)

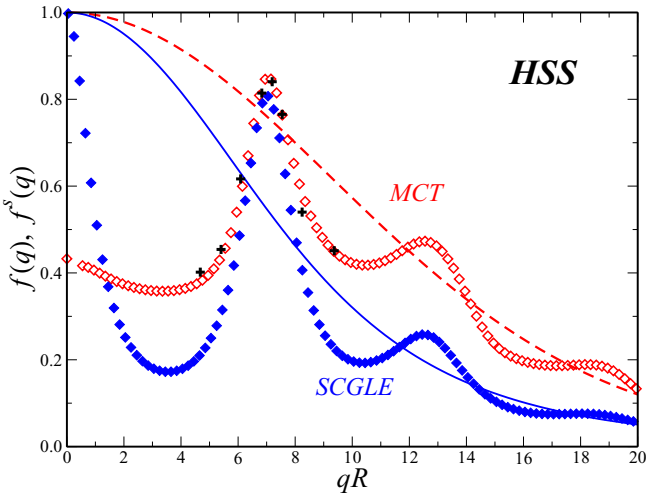

FIG. 1. Nonergodicity parameters $f^c(q)$ (symbols) and $f^{s,c}(q)$ (lines) for the hard-sphere (HS) system with PY structure factor, for MCT (open diamonds, dashed line, respectively) and SCGLE (filled diamonds, solid line) at their respective critical points. Cross symbols denote experimental data for $f^c(q)$ from Ref. [43].

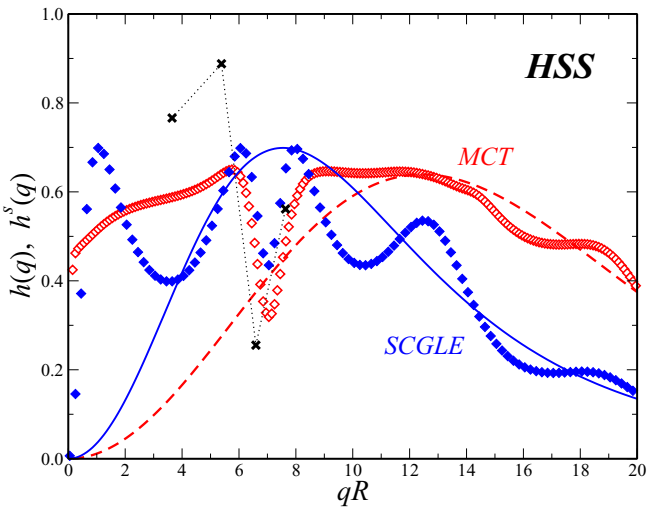

FIG. 2. Critical amplitudes $h(q) = H(q)/S(q)$ (symbols) and $h^s(q) = H^s(q)$ (lines), for the HSS as predicted by MCT (open diamonds and dashed lines, respectively) and SCGLE (filled diamonds and solid lines), with the PY approximation for the static structure factor. Cross symbols represent experimental estimates of $h(q)$ from Ref. [44].

approximation [33] provides an analytical parameter-free estimate. We will in the following discuss the standard normalized correlation functions, $\phi(q,t) = \Phi(q,t)/S(q)$.

Figure 1 shows the results for the nonergodicity parameters (NEPs) $f^c(q) = F^c(q)/S^c(q)$ and $f^{s,c}(q) = F^{s,c}(q)$ obtained from both MCT and SCGLE for the HS model and evaluated at their respective critical points. For the SCGLE calculations, the cutoff parameter was chosen as $k^c = 12.1957$ [corresponding to the position of the second maximum in $S(q)$ at the transition density]. With this choice, both theories predict glass-transition packing fractions that are very similar. We obtain $\varphi^c \approx 0.5143$ for SCGLE and $\varphi^c \approx 0.5158$ for MCT.

The NEPs shown in Fig. 1 display the standard behavior found in many glass-forming fluids: The collective $f^c(q)$ display oscillations as a function of wave number q that are roughly in phase with those of $S(q)$, indicating medium-range order induced by the hard-core repulsion. The different structure at $q \to 0$ of SCGLE that was pointed out above is clearly seen by an increase of the respective $f^c(q)$ to unity that sets in for $qR \lesssim 3$. The MCT values of $f^c(q)$ instead approach a limiting value $f^c(0) \approx 0.42$ in this regime. Experimentally, the $f^c(q)$ have been obtained from dynamic light scattering on colloidal hard-sphere-like suspensions [43]; these data are included in Fig. 1 as cross symbols.

In both theories, $f^s(q)$ is a monotonically decaying function of q that interpolates through the oscillations of $f(q)$. The width of the $f^s(q)$-versus-q curve is a measure of the localization length of a tagged particle and thus a measure of the average size of nearest-neighbor cages. SCGLE predicts a somewhat narrower $f^s(q)$-versus-q curve, corresponding to less tight localization in the glass. The dynamic order parameter of SCGLE is obtained as $\bar{\zeta} \approx 78.89/R^2$; using the definition of the localization length, we obtain $r_c = 1/\bar{\zeta} \approx 0.113R$ from SCGLE. The corresponding MCT value has to be obtained by a separate calculation of the mean-squared displacement from the $q \to 0$ limit of Eq. (9); one obtains $r_c = 1/\sqrt{\lim_{t\to\infty} \lim_{q\to 0} q^2 m^s(q,t)}$, and for the numerical results of Fig. 1 the value $r_c \approx 0.0745R$. In both cases, r_c amounts to a fraction of about 10% of the particle diameter. This is often referred to as the Lindemann criterion for melting.

The critical amplitudes $h(q) = H(q)/S(q)$ obtained from Eq. (18) are shown in Fig. 2. (We set the normalization to $\mathcal{N} = 1$ here.) Again the functional shapes obtained from the two theories are reasonably similar; the MCT results have been discussed in detail [20]. Generically, $h(q)$ shows a narrow dip around the q value where $f^c(q)$ is maximal: when the nonergodicity plateau is large, the next-order asymptotic decay needs to have a smaller amplitude because the correlation function is bounded.

The major differences between SCGLE and MCT again are a slower decay of the curves with q in MCT, and the emergence of an increase towards small q in the collective part in SCGLE. Here, due to the definition of $H(q)$ involving terms $S(q) - F(q)$, the SCGLE result obeys $h(q) \to 0$ for $q \to 0$, which results in an additional peak around $qR = 1$. Again, the MCT result for the collective dynamics approaches a nonzero constant at $q \to 0$. Recently, a careful analysis of data from dynamic light scattering allowed an experimental estimate of $h(q)$ for the HSS close to the glass-transition point [44]; the corresponding data are displayed in Fig. 2 as cross symbols.

We now illustrate the scaling behavior of the correlation functions, $\phi(q,t)$ and $\phi^s(q,t)$, in the vicinity of the glass transition in both SCGLE and MCT. Figure 3 shows these functions for a set of exemplary wave numbers around the first peak in the static structure factor. At and above the glass transition (solid and dashed lines in the figure), the decay towards a nonzero long-time limit given by $f(q)$, is seen. Close to but below the glass transition (square and circle symbols), the correlators decay to zero on a timescale that gradually diverges as $\varphi \to \varphi_c$ from below, opening an increasing time window where the correlation functions remains close to the

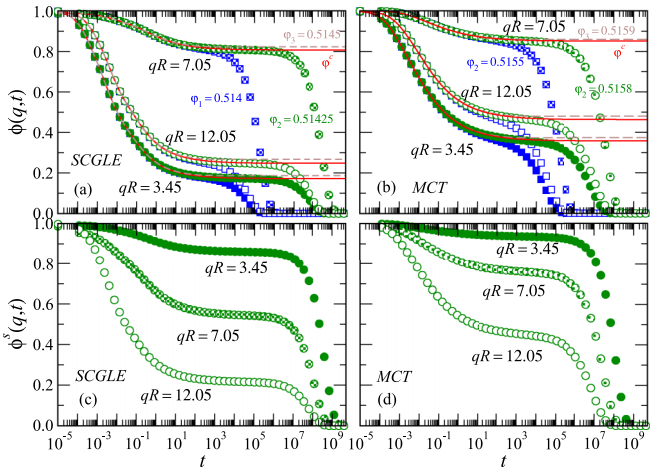

FIG. 3. Correlation functions $\phi(q,t)$ and $\phi^s(q,t)$ close to the glass transition of the monodisperse HS system using PY static structure, as predicted by SCGLE [left: panels (a) and (c)] and by MCT [right: panels (b) and (d)]. Results are shown for four different densities and three wave numbers: $q\sigma = 3.45$ (filled symbols), 7.05 (shaded symbols), and 12.05 (empty symbols) as labeled. For SCGLE, the densities are $\varphi_1 = 0.514$ (squares), $\varphi_2 = 0.51425$ (circles), $\varphi = 0.51425742 \approx \varphi^c$ (solid lines), and $\varphi_3 = 0.5145$ (dashed lines); for MCT: $\varphi_1 = 0.5155$, $\varphi_2 = 0.5158$, $0.5158357 \approx \varphi^c$, and $\varphi_3 = 0.5159$.

plateau values $f^c(q)$. These plateau values depend on the wave number, and so does the shape of the final relaxation towards zero in the fluid.

As anticipated from Eq. (22), all curves for a given density can be scaled on top of each other. We exemplify this in Fig. 4

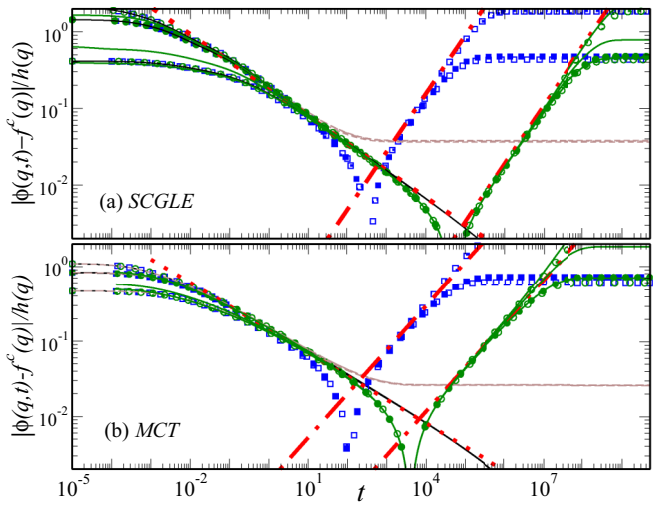

FIG. 4. Correlation functions from Fig. 3 shown as $|\phi(q,t) - f^c(q)|/h(q)$ in order to emphasize the scaling laws in SCGLE (top panel) and MCT (bottom panel). Dotted (red) lines show the corresponding critical decay laws $(t/t_0)^{-a}$, and dash-dotted (red) lines indicate the von Schweidler laws $\sim -(t/t_\sigma)^b$ where applicable (using $a = 0.3545$, $b = 0.7628$, and $t_0 = 0.008$ for SCLGE; $a = 0.312$, $b = 0.5845$, and $t_0 = 0.002$ for MCT). Symbols correspond to the collective correlation functions $\phi(q,t)$, while (green) solid lines indicate the tagged-particle correlation functions $\phi^s(q,t)$.

by demonstrating the asymptotic collapse to a q-independent scaling function for the quantity $|\phi(q,t) - f^c(q)|/h(q)$. Here, the critical decay law $\sim(t/t_0)^{-a}$ clearly emerges (dotted lines in the figure), although the time window where the correlators follow this law depends both on q and on the packing fraction. For $\varphi < \varphi_c$, the timescale t_σ sets the timescale where the correlators cross over to the von Schweidler law, $\sim -(t/t_\sigma)^b$; this is shown by dot-dashed lines in the figure. A further rescaling by $t \mapsto \hat{t} = t/t_\sigma$ would collapse the functions $|\phi(q,t) - f^c(q)|/h(q)\sqrt{|\sigma|}$ also in this regime; this has been discussed at length in the context of MCT [20,21] and shall not be repeated here. Similarly, for $\sigma > 0$ all the correlators cross over to a final plateau that, in the scaled representation of Fig. 4 to first order, depends only on σ, i.e., the distance to the transition.

Thus, the qualitative scenario that emerges is identical for SCGLE and MCT in the HSS. Because the dynamical exponents close to the glass transition are nonuniversal, the values obtained from SCGLE and MCT also slightly differ. For the exponent parameter λ, we obtain $\lambda \approx 0.628$ ($e \approx 0.999666$) for SCGLE and $\lambda \approx 0.734$ ($e \approx 0.999604$) for MCT. This corresponds to ($a \approx 0.3545$, $b \approx 0.7628$) and ($a \approx 0.312$, $b \approx 0.5845$), respectively. This can be compared to estimates $a = 0.3 \pm 0.08$ and $b = 0.52 \pm 0.04$ that were recently obtained by studying the numerical derivatives of experimentally measured correlation functions [44]. While that value of a agrees within error bars with both theories, the value of b is closer to the MCT prediction.

The timescale t_0 that characterizes the nonasymptotic short-time part of the relaxation was determined numerically by matching the critical decay law to the full solutions, with the chosen parameters we obtain $t_0 = 0.008$ (0.002) for SCGLE (MCT). The small but subtle difference in the value of t_0 indicates that this timescale is not fixed by the free-diffusion matrix only and thus a nontrivial quantity to determine.

Figure 4 also demonstrates that the validity of the scaling law depends on the wave number q. It can further be seen that, while the scaling law demands that all correlators decay from the plateau on the same timescale t'_σ that is independent of q, the relevant structural-relaxation time that one extracts from the correlation function itself varies with q. This variation amounts to a factor of 10 already for the q-range shown in Figs. 3 and 4.

It is known empirically that, close to the glass transition, the long-time part of the relaxation functions can be well described by a stretched-exponential law, $\phi(q,t) \approx A_q \exp[-(t/\tau_q)^{\beta_q}]$, where the structural-relaxation time τ_q and the stretching parameter β_q depend on the wave number. In the limit $q \to \infty$, it has been shown within the framework of MCT that the stretched-exponential law (also known as "Kohlrausch law") with $\beta_{q\to\infty} = b$ arises as a limit law [45]. The proof rests on the emergence of the universal scaling laws and the fact that at large q, the vertices decay to zero quickly enough. This leads to the statement that $f^c(q) \to 0$ in the limit $q \to \infty$, and that $H(q)/f^c(q)$ does not grow faster than q. In SCGLE, in fact, from Eqs. (14) and (20) one obtains $f^c(q) \sim 1/q^2$ and that $H(q)/f^c(q)$ is bounded by a constant as $q \to \infty$. The proof of Ref. [45] thus can be adapted, so that the stretched-exponential law also emerges as an asymptotic limit law for $q \to \infty$ in SCGLE.

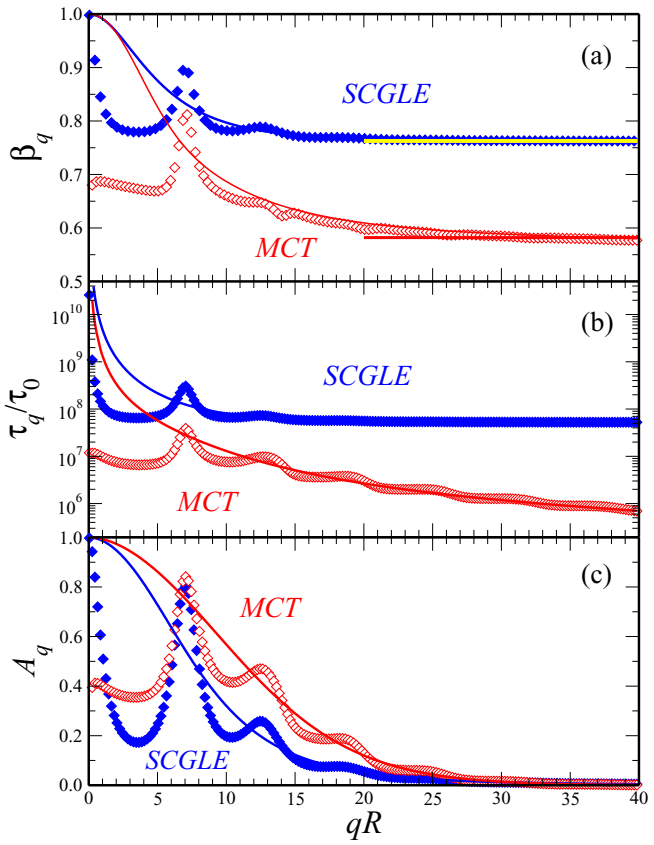

FIG. 5. Parameters of stretched-exponential fits, $\phi(q,t) \approx A_q \exp[-(t/\tau_q)^{\beta_q}]$, to the long-time part of the correlation functions obtained from SCGLE (filled symbols) and MCT (open symbols). Fits were obtained for the packing fractions $\varphi = 0.51425$ (SCGLE) and $\varphi = 0.5158$ (MCT), respectively, in the range $t \in [10^4{:}10^{10}]$. Lines are the parameters obtained from fits to the corresponding tagged-particle correlation function $\phi^s(q,t)$. Horizonal lines in the upper panel indicate the values of the von Schweidler exponent, $b = 0.7628$ (SCGLE) and $b = 0.5845$ (MCT), respectively.

The situation is exemplified in Fig. 5, where we show the fit parameters A_q, τ_q, and β_q, obtained from stretched-exponential fits to correlators of SCGLE and MCT close to their respective glass transitions. Some care has to be taken in the choice of the fit region, in order to avoid overfitting the crossover from the microscopic short-time relaxation to the long-time structural relaxation. As a cross-check, we verify that the amplitudes A_q closely match the expected plateau values $f^c(q)$ obtained from the solution of the theory. That this is indeed the case for our fits can be seen from comparing the lower panel of Fig. 5 with Fig. 1.

The relaxation times τ_q as a function of q vary roughly in phase with the amplitudes, and hence with the static structure factor $S(q)$ for the collective dynamics. The relaxation time obtained from fitting the tagged-particle correlation functions in the HS case interpolate between the oscillations corresponding to the collective relaxation dynamics for wave numbers $qR \gtrsim 7$, i.e., for q exceeding the position of the first peak in $S(q)$. At low q, the tagged-particle relaxation time $\tau_q^s \sim 1/q^2$, for both SCGLE and MCT, which reflects the existence of a diffusion pole in the hydrodynamic limit. As discussed above in connection with the $f^c(q)$, SCGLE copies this behavior also to the collective relaxation dynamics as a consequence of the Vineyard approximation. This reflects an (unphysical, in the present monodisperse system) slow collective-diffusion pole. The more involved structure of the MCT memory kernel does not suffer from this issue. At large q, a further qualitative difference between SCGLE and MCT becomes evident: within SCGLE, the relaxation time approaches an asymptotic constant, $\tau_{q\to\infty} \to$ const, whereas in MCT it approaches a decaying function of increasing q.

The stretching exponents β_q (top panel of Fig. 5) again show the oscillations in q that are inherited from the static structure of the system. Again, in the low-q limit, SCGLE and MCT differ qualitatively for the collective dynamics, and this difference is due to the simplification of the memory kernel present in SCGLE. For the tagged-particle dynamics, $\beta_{q\to 0} \to 1$ holds, and again this reflects the correct hydrodynamic diffusion pole, where density fluctuations decay exponentially. For both theories, the data are compatible with the expected large-q behavior $\beta_{q\to\infty} \to b$, although in MCT there appear some small deviations, possibly due to small numerical inaccuracies.

The difference in the power-law exponents obtained from MCT and SCLGE is small, and thus the quantitative differences between the two theories that are shown for example in Fig. 4 are unlikely to be assessed in simulation or experiment: the asymptotic power laws are valid over limited windows in time, and preasymptotic corrections to the scaling law can be strong (depending on the observable and in particular the wave number). Additional relaxation mechanisms not accounted for in either theory are present in experiment and simulation and cause deviations also at long times and close to the ideal glass-transition point where the asymptotic laws should hold best. This makes a robust determination of the scaling laws from data notoriously difficult. To assess systematic errors made by the theories, one would also need to understand better the way in which approximations used for $S(q)$ alter the numerical values. The effect of such approximations can be larger than the differences discussed in connection with Fig. 4, which we therefore consider irrelevant for practical purposes. However, a systematic study of the q-dependence of relaxation times and of the shapes of structural-relaxation spectra could probe the differences between MCT and SCLGE that are highlighted by Fig. 5.

B. Generalized Gaussian-core model (GCM4)

An illustrative example concerning the different treatment of collective and self-dynamics in MCT and SCGLE is provided by the generalized Gaussian core model with exponent 4 (GCM4). One assumes the (bounded) pair potential

$$V(r) = \varepsilon e^{-(r/R)^4}, \tag{27}$$

where ε is the energy in units of the thermal energy, and $R = 1$ sets the unit of length. The GCM4 has been studied in the context of ultrasoft colloids such as star-polymer solutions, and it is a model system that captures the occurrence of a cluster phase [46–48], i.e., a phase where particles can overlap with each other such that a further increase in density does not change the interparticle spacing but rather the number of

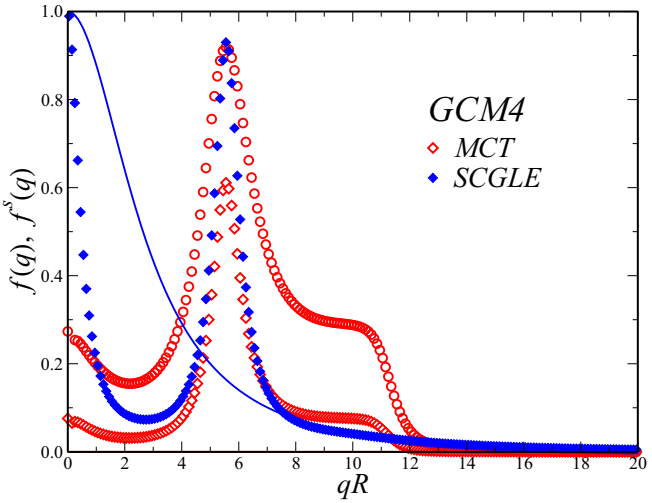

FIG. 6. Nonergodicity parameters $f^c(q)$ (symbols) and $f^{s,c}(q)$ (line) for the generalized Gaussian core model GCM4 using the MSA structure factor, for energy $\varepsilon = 1$, as obtained within MCT (open diamonds) and SCGLE (filled diamonds) at their respective glass-transition points. Within MCT, $f^{s,c}(q) = 0$. Open circles show the MCT $f(q)$ at the "type A" transition where $f^s(q)$ starts to increase continuously from zero.

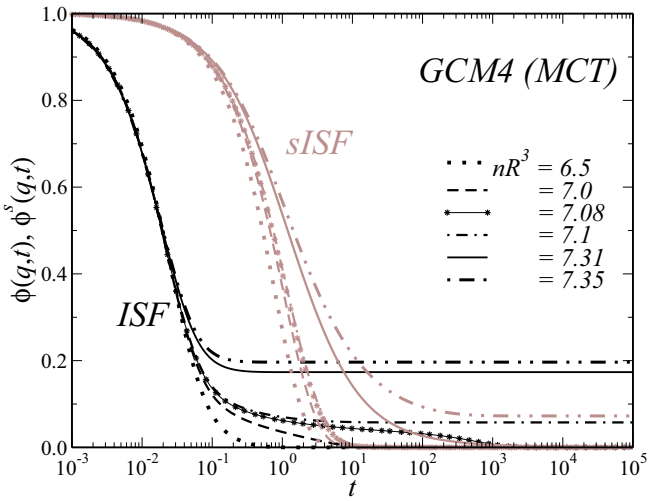

FIG. 7. Normalized collective density correlation functions $\phi(q,t)$ and tagged-particle density correlation functions $\phi^s(q,t)$, for the GCM4 model as predicted by MCT for fixed $\varepsilon = 1$, at wave number $qR = 1.4$ and number densities $nR^3 = 6.5$, 7.0, 7.08, 7.1, 7.31, and 7.35 as indicated.

particles sharing the same average location. A cluster glass phase has been found specifically for the GCM4 model using some polydispersity in size to avoid crystallization [49]. In these cluster phases, the collective dynamics of the density fluctuations is slow, but hopping-like single-particle motion persists. This is quite different for the Gaussian core model, where the glassy relaxation shows stronger coupling between collective and self-motion than usual [50,51]. Mixed states of the kind observed in the GCM4 (i.e., arrested collective dynamics with mobile single-particle dynamics) have been discussed extensively in the context of mixtures, in both MCT and SCGLE. For one-component systems they are less prominent and have not yet been reported in theory (not counting systems with frozen disorder [52,53]).

A good approximation of the static structure of the GCM4 for not too low temperature is provided by the mean-spherical approximation (MSA), where one sets $c(r) = -\beta V(r)$ outside the hard core [33]. Since the GCM4 has no hard core, the MSA here amounts to setting $c(q) = -\beta V(q)$ for all q, where the Fourier transform $V(q)$ of $V(r)$ is obtained in terms of generalized hypergeometric functions. The model then has two control parameters, *viz.*, the inverse temperature ε (setting the thermal energy to unity) and the density n.

Nonergodicity parameters $f(q)$ and $f^s(q)$ obtained for the GCM4 at $\varepsilon = 1$ with both MCT and SCLGE are shown in Fig. 6. SCGLE, using again $k^c = 12.1957$ as above for the HSS, gives a glass transition at $n^c \approx 7.758134$ ($\lambda \approx 0.534$). While some qualitative features of $f^c(q)$ are as expected from the above discussion, it is remarkable that the f-versus-q curve, apart from the well-understood increase for $q \to 0$, shows only a single strong maximum. This expresses the fact that, contrary to the HSS, the glassy structure of the GCM4 model lacks the well-defined nearest-neighbor distance ℓ that expresses itself in oscillations of a period $\approx 2\pi/\ell$ in the Fourier transform.

MCT gives a glass transition at $n^c \approx 7.085247$ ($\lambda \approx 0.535$). But here, while $f^c(q) > 0$ indicates the usual discontinuous ("type B") glass transition, the tagged-particle nonergodicity parameters remain zero, $f^{s,c}(q) = 0$. Thus, MCT describes the arrest of collective density fluctuations in the GCM4 model where tagged-particle motion remains ergodic. Further increasing the density, a second transition is encountered at $n^{c,s} \approx 7.31$, where $f^s(q) \neq 0$ arises but the $f(q)$ remain continuous. This latter is not a transition signaled by a critical eigenvector in $C[H]$, but rather in the analogous equation or $C^s[H^s]$ which in MCT is separate. The tagged-particle nonergodicity parameters $f^{s,c}(q)$ increase continuously from zero, and since $f^s(0) = 1$ always has to hold, the $f^s(q)$-versus-q curve just above the second transition is a narrowly peaked function around $q = 0$. To this corresponds a localization length that diverges to infinity as one approaches the transition from the localized side. A more stringent investigation of the asymptotic behavior close to such "type A" transitions within MCT requires additional care [54] and is beyond the scope of the present paper. But to illustrate the generic scenario for the dynamical correlation functions, Fig. 7 shows MCT results for a set of densities that span the two transitions. The collective density correlators $\phi(q,t)$ show the two-step glass-transition scenario discussed above in connection with the HSS (albeit with untypically low plateau values for the wave number chosen in the figure). At the same time, the tagged-particle correlation functions $\phi^s(q,t)$ (dashed lines in Fig. 7) remain decaying to zero in the long-time limit; they also do not show an indication of a two-step relaxation scenario. As the type A transition is crossed, no peculiar behavior is seen in the collective dynamics (top two curves in the figure), while the tagged-particle correlation function develops a finite long-time limit that rises continuously from zero.

The separation of the collective glass transition and the single-particle localization transition obtained from MCT

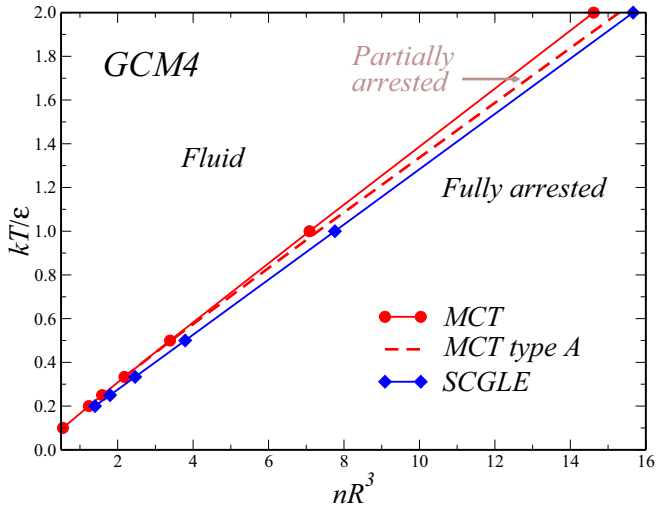

FIG. 8. Glass-transition diagram of the generalized Gaussian core model GCM4 using the MSA structure factor, obtained from MCT (red) and SCGLE (blue), in the plane spanned by number density n and thermal energy relative to the potential height, kT/ε. For MCT, two separate lines are shown for the arrest of collective (solid line with symbols) and tagged-particle (dashed line) density fluctuations.

depends on the choice of ε. As one increases this parameter, the two transition points merge (for example, for $\varepsilon = 5$, the single transition point $n^c \approx 1.2358$ is obtained in MCT). This is intuitively expected, since for large ε, the energy of thermal fluctuations is no longer sufficient to surmount the energy barrier posed by the potential, and the system approaches hard-core behavior. (But note that the quality of the MSA approximation for the static structure should be more carefully evaluated in this limit.) Figure 8 shows the glass-transition curves obtained for the GCM4 from MCT and SCGLE in the $(n, 1/\varepsilon)$-plane. Both theories predict the intuitively expected trend (i.e., arrest at higher density for higher temperature). Let us note that the shape of the $f^c(q)$-versus-q curves discussed in conjunction with Fig. 6 does not change qualitatively with ε, and for both theories the height of the nonergodicity parameters simply increases somewhat with increasing ε. Also the values of λ do not change appreciably: They slightly increase with increasing ε for SCGLE but decrease for MCT; a clear physical interpretation of this effect is unknown to us. The values for $\varepsilon = 1$ are close to $\lambda = 1/2$ for which one would get a von Schweidler exponent of $b = 1$, indicating nonstretched exponential structural relaxation.

One notes the emergence of a "cluster glass" phase within MCT at high temperatures (area between the solid and dashed MCT lines in the figure) with collective arrest but long-range tagged-particle motion. A qualitative comparison of our MCT results to the simulation data of the cluster glass phase of Ref. [49] is beyond the scope of this paper, but we find it remarkable that the theory reproduces the peculiar behavior of this permeable-particle model. A similar decoupling of tagged-particle and collective motion at high temperatures in the dynamics of a bounded-potential model can also be identified in recent simulations of particles interacting with a generalized Hertzian potential [55].

V. BINARY HARD-SPHERE MIXTURES (BHSMS)

To discuss more clearly the different role played by the collective and the tagged-particle dynamics close to the glass transition, we now turn to the model system of binary hard-sphere mixtures (BHSMs). For this, let us consider $N = N_b + N_s$ (big and small) spheres of diameters R_b and R_s and interacting through the HS potential. The three control parameters of this system can be expressed in terms of the overall packing fraction φ, the relative packing fraction of the second species $\hat{x}_s \equiv \hat{x} = \varphi_s/\varphi$, and the size ratio $\delta = R_s/R_b$. We use the convention that $\delta < 1$, and fix the unit of length by the size of the larger particles, R_b. The concentration $\hat{x}$ sets the number concentrations $x_s \equiv x = N_s/N$ and $x_b \equiv 1 - x$ of the two species. For convenience, let us denote the conversion rule that follows from observing

$$\hat{x}_b + \hat{x}_s/\delta^3 = [x_b + x_s\delta^3]^{-1}, \tag{28a}$$

viz.,

$$\hat{x} = \frac{x\delta^3}{1 - x(1-\delta^3)}, \quad x = \frac{\hat{x}/\delta^3}{1 - \hat{x}(1 - 1/\delta^3)}. \tag{28b}$$

In the numerical calculations for the BHSM, we determine the cutoff parameters k_α^c used in SCGLE [see Eq. (4b)] to coincide with the first minimum after the main peak in $S_{\alpha\alpha}(q)$. This is a convenient procedure to account for the change in length scale as one crosses over from $\hat{x} = 0$ to $\hat{x} = 1$ for $\delta \ll 1$. Note that this gives slightly different results for φ^c and λ in the monodisperse case when compared to the HS results presented above. We also adopt a different discretization of the q-space integrals: following Ref. [56] we use $M = 1000$ points with $\Delta q = 0.4/R_b$.

For size ratios δ close to unity, both theories essentially give the same result: depending on concentration $\hat{x}$, only small variations in φ^c and the related quantities result. The typical scenario observed in both approaches for $\delta \lesssim 0.6$ is a fluidization by mixing, causing $\varphi^c(\hat{x})$ to increase with respect to the monodisperse hard-sphere value ($\hat{x} = 0$) such that the φ^c-versus-$\hat{x}$ curve exhibits an intermediate maximum. Let us mention that MCT also predicts a regime of vitrification by mixing for δ close to unity, in agreement with computer-simulation results [57]. For $\delta = 0.8$, for instance, the MCT φ_c-versus-$\hat{x}$ curve has a minimum [38], and for $\delta = 0.7$ a curve with both a maximum and a minimum emerges. This nonmonotonic trend as a function of size ratio is not reported within SCGLE [18].

Figure 9 displays the predictions of the SCGLE (filled diamonds) and MCT (open diamonds) corresponding to the case $\delta = 0.5$ that is representative for the ordinary "fluidization-by-mixing" case. Two noteworthy quantitative differences between these theoretical predictions can be seen: first, the enhancement of φ_c due to mixing is more pronounced within SCGLE. Second, the position of the maximum in the φ_c-versus-$\hat{x}$ curve is shifted to lower $\hat{x}$ in SCGLE as compared to MCT. Within the latter, the strongest effects on the critical concentration are typically found when both species contribute roughly equally to the overall packing (by volume); within SCGLE, no intuitive rule emerges in this sense (note, however, that the small particles already dominate by number

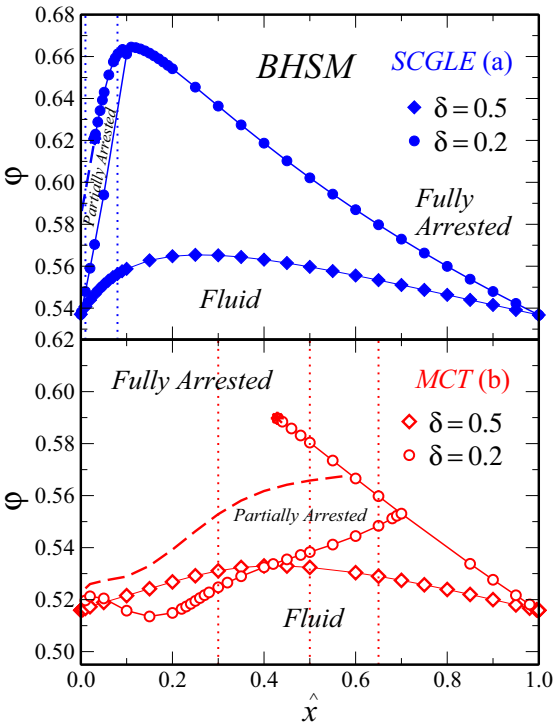

FIG. 9. Glass-transition points of the binary-hard sphere model for size ratios $\delta = 0.5$ (diamonds) and $\delta = 0.2$ (circles), evaluated within SCGLE (top panel; filled symbols) and MCT (bottom panel; open symbols), as functions of small-particle volumetric concentration $\hat{x}$. Lines with symbols represent discontinuous (type B) transitions, whereas dashed lines indicate continuous transitions (type A). Stars indicate endpoint singularities of type B transition lines (exponent parameter $\lambda = 1$). Dotted vertical lines indicate cuts of constant $\hat{x}$ that are considered in Figs. 11–14.

concentration, x, for the maximum in the φ_c-versus-$\hat{x}$ curve also within SCGLE).

In the following we shall be concerned with smaller size ratios. Figure 9 also shows the glass-transition points for mixtures with $\delta = 0.2$ as obtained from both theories (filled and open circles), which exemplifies the typical scenario for very size-disparate mixtures. Both approaches predict glass-glass transitions to occur below a certain threshold $\delta \lesssim 0.4$ [18,56]. In essence, for sufficiently large size asymmetry, the small species can distinguish a glass whose structure is governed by the large particles (with interdispersed small particles), from a glass whose structure emerges smoothly from that of the small-particle monodisperse glass (with embedded big particles). If the length scales controlling these glassy structures (set by δ) are sufficiently different and both species contribute significantly to dynamical arrest (intermediate $\hat{x}$ for MCT, intermediate x for SCGLE), an increase in overall packing fraction triggers first the transition from the fluid to the large-particle glass, and then, at a higher packing fraction, from the large-particle glass to the small-particle glass. A typical signature of this idealized glass-glass transition is a discontinuous jump in mechanical moduli. As shown in Fig. 9, for $\delta = 0.2$ the window of two glass transition extends from $\hat{x} \approx 0.4$ to $\hat{x} \approx 0.7$ in MCT. For SCGLE, in contrast, this window appears narrower and extends only from $\hat{x} \approx 0.03$ to $\hat{x} \approx 0.1$. At the large-$\hat{x}$ end of this window, the two transition lines that extend from $\hat{x} = 0$ and $\hat{x} = 1$, respectively, meet in a crossing point.

For the size ratio $\delta = 0.2$, the transition line extending from $\hat{x} = 0$ is one where only the big particles freeze. Within MCT, this implies that, while all collective correlation functions arrest to nonzero nonergodicity parameters, the tagged-particle correlation function associated with the small species still decays. Within SCGLE, the same is true, but additionally the collective propagator matrix $\mathbf{\Psi}$ develops zero entries (as discussed above in Sec. III A) for Ψ_{ss}. In both cases, since one can continuously cross over from this partially arrested glass to the fully arrested glass that both theories predict for large $\hat{x}$ (or x) and large φ, this implies that there appears a further transition line where small-particle motion arrests. This transition from the partially arrested glass to the fully arrested one is a continuous transition in the sense that there the relevant nonergodicity parameters rise continuously from zero. These type A or localization transitions are shown as dashed lines without symbols in Fig. 9; hence the region between these dashed and the surrounding solid transition lines demarks the region of the partially arrested glass.

Here, a qualitative difference between MCT and SCGLE emerges regarding the topology of the kinetic-arrest diagram: within MCT, the localization line that determines arrest of the self-motion of small particles in the glass formed by the large particles is essentially separate from the collective glass-transition lines. In SCGLE, however, this localization lines necessarily emerges from the endpoint of the small-particle glass-transition line (that extends from $\hat{x} = 1$).

Note that the endpoint of the small-particle glass-transition line does not generically coincide with the crossing point of the two collective glass-transition lines. Mathematically, the transition lines drawn in Fig. 9 are the physically relevant parts of a bifurcation diagram with two lines of A_2 singularities that cross and each end at a "higher-order singularity" (A_3 singularity indicated by $\lambda = 1$) of which just one bears physical significance [11]. By a further tuning of parameters it can occur that these endpoints meet (and thus coincide with the crossing point, in an A_4 singularity). These features have been discussed within MCT at length in the context of the square-well model [58], the simplest known microscopic model of physical relevance for which MCT exhibits these higher-order singularities. The topology of the bifurcation scenario (in a state space with three relevant control parameters) is robust, and thus it emerges from both MCT and SCGLE, although the distinction between the crossing point and the endpoint singularity appears to have been overlooked in previous SCGLE literature.

The values of the exponent parameters along the transition lines displayed in Fig. 9 and discussed above are shown in Fig. 10. The generic trend is that MCT predicts slightly larger values of λ, but as discussed above these differences translate to small differences in the critical exponents that are hard to distinguish in experiment or simulation. A quantitative difference, however, becomes manifest in the location of the endpoint singularity where $\lambda \to 1$, regarding the volumetric concentration $\hat{x}$ of the small particles. In line with the discussion above, SCGLE predicts much smaller $\hat{x}$ to be sufficient to trigger the higher-order singularity. In the vicinity

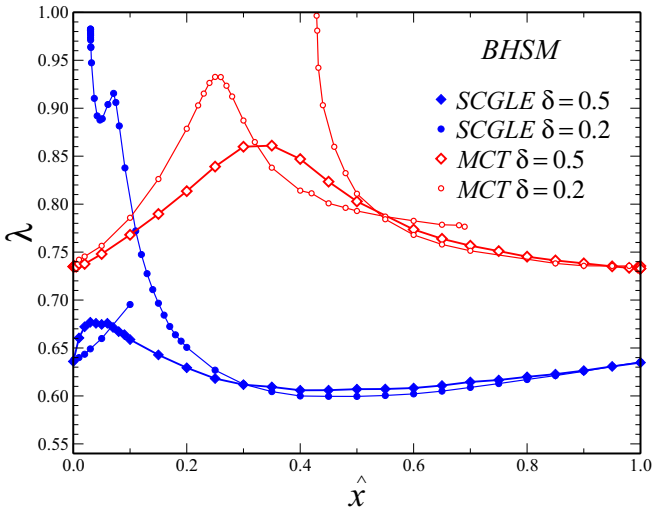

FIG. 10. Exponent parameter λ of the binary-hard sphere mixtures for size ratios $\delta = 0.5$ (diamonds) and $\delta = 0.2$ (circles) as functions of small-particle concentration $\hat{x}$ along the transition lines shown in Fig. 9, for SCGLE (filled symbols) and MCT (open symbols). In the SCGLE branch, the value $\lambda = 1$ is not reached within the precision of our numerics.

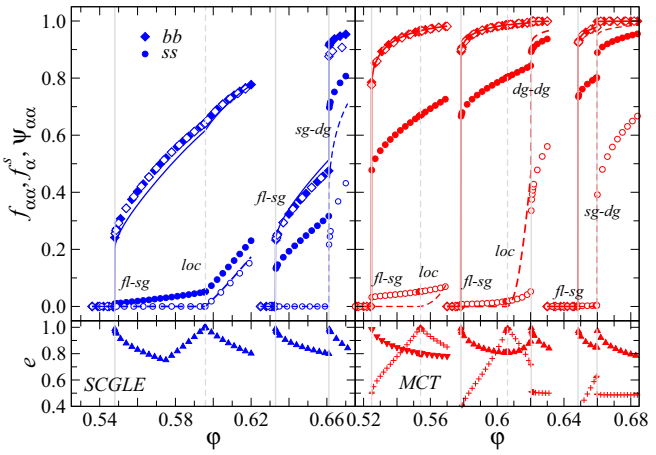

FIG. 11. Top panels: nonergodicity parameters $f_{\alpha\alpha}(q) = F_{\alpha\alpha}(q)/S_{\alpha\alpha}(q)$ (b: filled diamonds; s: filled circles) and corresponding long-time limits of the propagator, $\psi_{\alpha\alpha}(q) = [\boldsymbol{F}(q) \cdot \boldsymbol{S}^{-1}(q)]_{\alpha\alpha}$ (open symbols) as functions of total packing fraction φ along cuts of constant $\hat{x}$ for $\delta = 0.2$, for fixed wave number $qR = 12.2$. Left panel: SCGLE for $\hat{x} = 0.01$ (left) and $\hat{x} = 0.08$ (right). Right panel: MCT for $\hat{x} = 0.3$ (left), $\hat{x} = 0.5$ (shifted in φ by 0.04 for clarity; middle), and $\hat{x} = 0.65$ (shifted by 0.10; right). Solid and dashed lines indicate the tagged-particle nonergodicity parameters $f^s_\alpha(q)$. (Some open and closed triangle symbols overlap due to numerical closeness.) Bottom panels: Maximum real eigenvalues relevant for the asymptotic expansion (triangle symbols). For MCT, also the separate eigenvalues for the tagged-particle correlator expansion are shown (crosses).

of the endpoints, different asymptotic decay laws apply, as formally the exponent of the critical decay law approaches zero, $a \to 0$. There then appear logarithmic decay laws, as has been worked out in detail for MCT [59–61] and applies *mutatis mutandi* for SCGLE. Such logarithmic decay laws cause the correlation functions for a range of parameters near the endpoint singularity to appear as anomalously stretched in their decay, and this signature can be identified in experiment or simulation.

To elucidate the different types of glass transitions that are predicted for size-disparate HS mixtures, we show in Fig. 11 the nonergodicity parameters at a fixed q value, as a function of increasing total packing fraction φ along various cuts through the state diagram of constant $\hat{x}$. (These cuts are illustrated by vertical dotted lines in Fig. 9.) For ease of comparison, we show the *ad hoc* normalized values $f_{\alpha\beta}(q) = F_{\alpha\beta}(q)/\sqrt{S_{\alpha\alpha}(q)S_{\beta\beta}(q)}$. As φ is increased from the fluid state at low packing fraction to the fully arrested "double-glass" state at high packing fraction, three qualitatively different scenarios can be distinguished, two of which are predicted to occur within SCGLE and also MCT, and a third that is specific to MCT.

Table I summarizes the schematic behavior of the nonergodicity parameters and the long-time limits of the propagators along the cuts considered in Fig. 11. We discuss the three

TABLE I. Qualitative behavior of the nonergodicity parameters $f_{\alpha\alpha}(q)$ of the collective dynamics, the tagged-particle nonergodicity parameters $f^s_\alpha(q)$, and the propagator long-time limits $\Psi_{\alpha\alpha}(q)$ at the different glass transitions. Table entries indicate the change in the respective quantity as follows. +: jump discontinuity; (+): typically small jump discontinuity; 0: remains zero; /: kink; −: no effect; empty: does not occur in the theory. The different transitions are as follows, with typical $\hat{x}$ values given for the $\delta = 0.2$ transition diagram. fl–sg/sg–dg: fluid to single glass, followed by glass-glass transition from single to double glass (SCGLE: $\hat{x} = 0.08$; MCT: $\hat{x} = 0.65$); fl–sg/loc: fluid to single glass, followed by localization transition to double glass (SCGLE: $\hat{x} = 0.01$; MCT: $\hat{x} = 0.3$); fl–sg/loc/dg–dg: fluid to single glass, localization transition of small particles, glass-glass transition (MCT: $\hat{x} = 0.5$).

	$f_{\rm bb}$		$f_{\rm ss}$		$f^s_{\rm b}$		$f^s_{\rm s}$		$\Psi_{\rm bb}$		$\Psi_{\rm ss}$	
Type	SCGLE	MCT	SCGLE	MCT	SCGLE	MCT	SCGLE	MCT	SCGLE	MCT	SCGLE	MCT
fl–sg/	+	+	+	+	+	+	0	0	+	+	0	(+)
loc	/	−	/	−	/	−	/	/	/	−	/	−
fl–sg/	+	+	+	+	+	+	0	0	+	+	0	(+)
sg–dg	+	+	+	+	+	+	+	+	+	+	+	+
fl–sg/		+		+		+		0		+		(+)
loc/		−		−		−		/		−		−
dg–dg		+		+		+		+		+		+

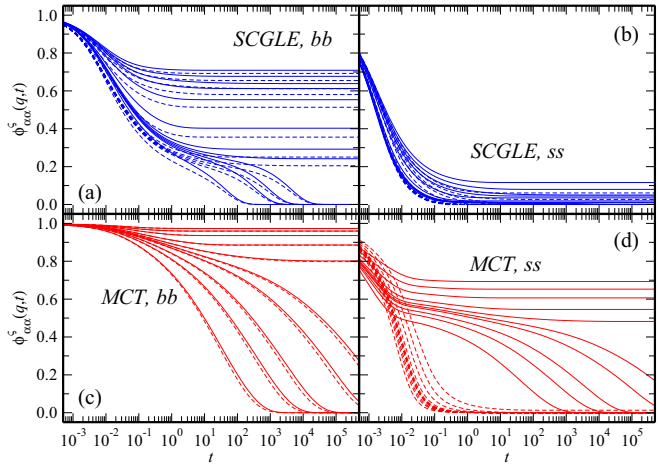

FIG. 12. Normalized collective, $\phi_{\alpha\alpha}(q,t)$ (solid lines), and tagged-particle, $\phi^s_\alpha(q,t)$ (dashed), density correlation functions at wave number $qR = 12.2$ for binary-hard sphere mixtures with size ratio $\delta = 0.2$, along a path of constant small-particle volumetric concentration $\hat{x}$ and increasing total packing fraction φ; for a path crossing the fluid–single-glass transition and a localization transition for the small particles (fl–sg/loc). Left panels show the large-particle correlators, $\alpha = \mathrm{b}$, right panels the small-particle correlators, $\alpha = \mathrm{s}$. (a) and (b): SCGLE for $\hat{x} = 0.01$ and $\varphi = 0.54$, 0.545, 0.546, 0.547, 0.548, 0.55, 0.56, 0.58, 0.59, 0.595, 0.6, and 0.605. (c) and (d): MCT for $\hat{x} = 0.3$ and $\varphi = 0.5$, 0.51, 0.515, 0.52, 0.522, 0.525, 0.53, 0.54, 0.55, and 0.56.

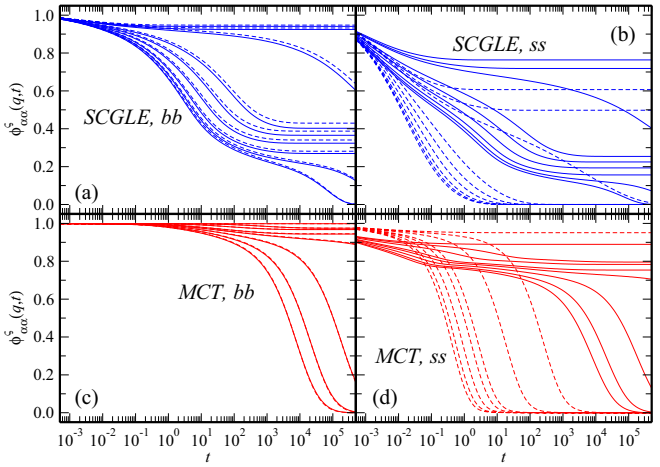

FIG. 13. Density correlation functions as in Fig. 12, but for a path crossing the fluid–single-glass transition followed by a single-glass–double-glass transition (fl–sg/sg–dg). Top panels: SCGLE for $\hat{x} = 0.08$ and $\varphi = 0.63$, 0.632, 0.635, 0.64, 0.645, 0.65, 0.66, 0.662, and 0.665. Bottom panels: MCT for $\hat{x} = 0.65$ and $\varphi = 0.54$, 0.542, 0.545, 0.548, 0.55, 0.555, 0.558, and 0.56.

generic cases below, together with the exemplary evolution of the density correlation functions with increasing packing fraction.

The first path of increasing φ, exemplified here by cuts at fixed low $\hat{x}$, crosses first a discontinuous transition from fluid to "single glass" (fl–sg), where the collective density fluctuations freeze, long-range transport of the large particles ceases, but long-range transport of the small particles remains possible. In other words, all the collective nonergodicity parameters $f_{\alpha\alpha}(q)$ jump from zero to finite values, and $f^s_{\mathrm{big}}(q)$ jumps to a finite value, but $f^s_{\mathrm{small}}(q)$ remains zero. This behavior is found in both MCT and SCGLE. Specific to SCGLE is the prediction that, in the single-glass state entered upon crossing this fl–sg transition, the propagator-long-time limit $\Psi_{\mathrm{ss}}(q)$ remains zero; in MCT it jumps to a finite value, albeit that value can be small, depending on the value of q. A further increase in packing fraction eventually causes arrest of the small particles, at a localization (loc) transition. Here, within SCGLE all relevant quantities exhibit a kink, i.e., a discontinuity in the slope. Within MCT, only the tagged-particle nonergodicity parameter associated to the small-particle motion, $f^s_{\mathrm{s}}(q)$, shows such behavior, while all other quantities remain unaffected. Figure 12 shows the evolution of the density correlation functions along the first path. The collective correlation functions $\phi_{\alpha\alpha}(q,t)$ show qualitatively the same behavior in both SCGLE and MCT. Owing to the differences in the respective state diagrams, the paths are evaluated at different small-particle concentrations $\hat{x}$ in the two theories; this causes notable quantitative differences in the numerical values of the nonergodicity parameters, in particular those associated to the small particles. Hence, the evolution of a two-step decay scenario around the fl–sg transition is hard to detect in the case of the small-particle correlators of SCGLE. As a result, the tagged-small-particle correlators and their collective counterparts remain numerically closer in SCLGE than in MCT, although they show the same qualitative difference regarding the absence respective presence of a two-step decay pattern.

The second exemplary path crosses the transition to the single glass (fl–sg), followed upon further increase of packing fraction by another discontinuous transition to a double glass (sg–dg). This latter is characterized by jump discontinuities in all long-time limits, i.e., jumps from one finite value to a higher one at all q. The qualitative behavior here is the same for both SCGLE and MCT. The dynamical scenario is exemplified by Fig. 13. Again, because the fl–sg/sg–dg scenario is present in MCT at much higher small-particle concentrations $\hat{x}$ than in SCGLE, numerical differences in the respective plateau values become evident. Apart from this, both theories show that for the large particles, collective and tagged-particle relaxation dynamics is nearly identical at the wave number chosen.

For the small particles, the tagged-particle correlation functions decay much faster than their collective counterparts; the latter decay as slowly as those associated to the large particles. This is the qualitative signature of the fluid–single-glass transition [56]. The strong decoupling in the relaxation of self- and collective correlations of the small particles has been verified in experiments and simulations on binary colloidal mixtures [27,28]. It is also known from noncolloidal glass formers and has been the basis to explain fast-ion conduction in sodium-silicate melts [29,30].

Around the single-glass–double-glass transition, a two-step decay scenario emerges for the tagged-small-particle correlator, signaling the approach to a discontinuous arrest transition for the small-particle dynamics that is different from the localization transition encountered along the first path. At

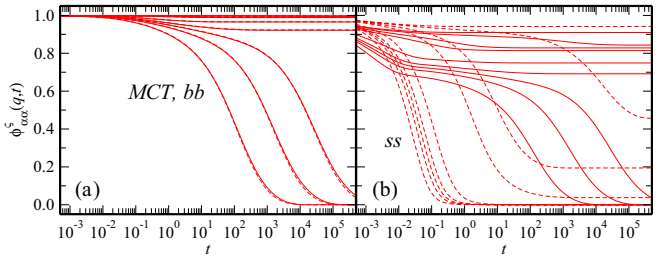

FIG. 14. Density correlation functions as in Fig. 12, but for a path crossing the fluid–single-glass transition, followed by a localization transition, followed by a double-glass transition (fl–sg/loc/dg–dg). MCT results for $\hat{x} = 0.5$ and $\varphi = 0.52$, 0.53, 0.535, 0.54, 0.55, 0.57, 0.575, 0.58, and 0.582.

the same time, the remaining correlation functions (that are already nonergodic on both sides of the sg–dg transition) show a two-step decay from one plateau to another finite one.

The third path, specific to MCT, arises because in this theory, the localization transition and the sg–dg transition do not emerge from singularities of the same stability matrix. They thus do not both end in the same higher-order singularity point and leave open the possibility of first crossing from the fluid into the single glass discontinuously (fl–sg), followed by continuous localization of the small particles (loc) into a fully arrested glass, followed by a further discontinuous transition where this fully arrested glass transforms into a more tightly packed one (dg–dg). The corresponding dynamical evolution is shown in Fig. 14. In essence, the evolution of the collective correlation functions is the same as that encountered along the second path, because the single-particle localization dynamics in MCT does not couple back to the collective quantities. Only the tagged-small-particle correlators show qualitative differences to the behavior exhibited by Fig. 13: around the double-glass transition, these correlators are already nonergodic, so that also for them, a two-step decay from one plateau to another finite one is observed.

Despite the differences regarding the arrest of small particles and the shape of the glass-transition diagram in the $(\hat{x}, \varphi)$ plane, many predictions of both theories again are rather similar when evaluated at similar concentrations $\hat{x}$. This is in particular true for the case where only double-glass states are predicted. We demonstrate this by a comparison of the nonergodicity parameters for the size ratio $\delta = 0.5$ in Fig. 15. Both SCGLE and MCT yield roughly similar $f^c_{\alpha\beta}(q)$ for the cases $\hat{x} = 0.2$ and $\hat{x} = 0.8$, taken as exemplary for the full state space. In contrast to the monodisperse case, even in the limit $q \to 0$, no strong differences are seen in the partial nonergodicity factors. This is due to the fact that the $q \to 0$ behavior reflects the presence or absence of conservation laws; the formulation of both theories in the case of mixtures rests on the partial number-density fluctuations, and these do not obey a separate momentum-conservation law. Thus, the corresponding partial nonergodicity parameters approach unity for $q \to 0$, just as the tagged-particle quantities. In this respect, the starting points from SCGLE and MCT (hinging respectively on the tagged-particle momentum fluxes and the collective ones) become quite similar.

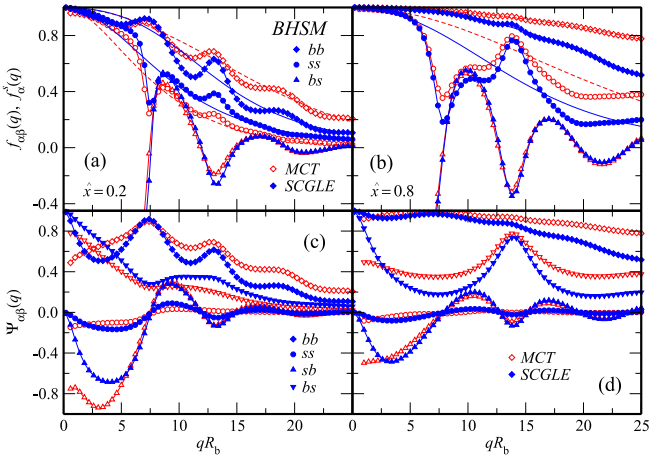

FIG. 15. Nonergodicity parameters for binary hard-sphere mixtures (PY closure) with size ratio $\delta = 0.5$. (a) and (c) Volume concentration of small particles $\hat{x} = 0.2$; (b) and (d) $\hat{x} = 0.8$. Top panels show the normalized nonergodicity parameters $f^c_{\alpha\beta}(q) = F^c_{\alpha\beta}(q)/\sqrt{S_{\alpha\alpha}(q)S_{\beta\beta}(q)}$, for SCGLE (filled symbols) and MCT (open symbols). Lines are the tagged-particle $f^{s,c}_\alpha(q)$ (solid: SCGLE; dashed: MCT). The three independent elements of the matrix are shown as labeled. The bottom panels show the propagator long-time limits $\Psi_{\alpha\beta}(q) = [\boldsymbol{F}^c(q) \cdot \boldsymbol{S}^{-1}(q)]_{\alpha\beta}$. All four elements are shown as labeled.

As expected, more notable differences arise in the nonergodicity parameters of the partially arrested glass. We exemplify this by the case $\delta = 0.2$ and $\hat{x} = 0.002$; this corresponds to a state point previously discussed in the context of SCGLE [18]. In Fig. 16 we show the nonergodicity parameters $f_{\alpha\beta}(q)$, $f^s_\alpha(q)$ (upper panel) and propagator long-time values $\Psi_{\alpha\beta}(q)$ (lower panel) for two overall packing fractions: one at the transition from the fluid to the partially arrested glass (left panels of the figure), and one slightly above the localization transition of the small particles, i.e., the transition from the

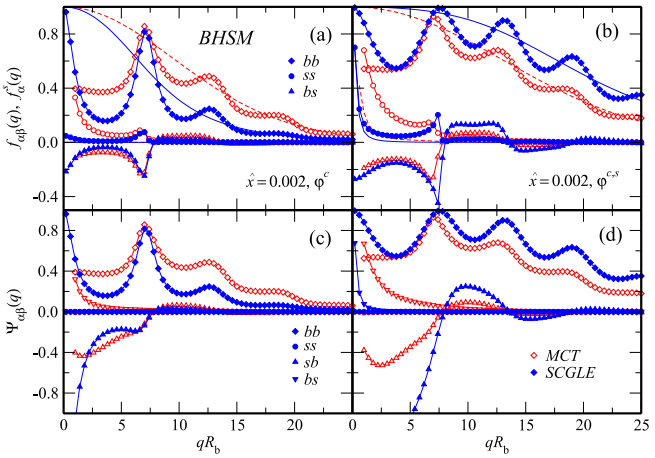

FIG. 16. Nonergodicity parameters for binary hard-sphere mixtures as in Fig. 15, but for size ratio $\delta = 0.2$ and small-particle concentration $\hat{x} = 0.002$. Evaluated (a) and (c) at the glass-transition point φ^c and (b) and (d) at a packing fraction slightly above the separate localization transition of the small particles.

partially arrested to the fully arrested glass (right panel). Again, at finite q both theories yield qualitatively similar predictions. In the limit $q \to 0$, differences are seen that are reminiscent of the monodisperse hard-sphere case discussed above. In fact, this is a surprising signature of the partially arrested glass that appears even in the collective nonergodicity parameters of MCT, although that theory *a priori* treats the tagged-particle motion as a fully separate problem: while for the fully arrested glass (cf. Fig. 15) the $q \to 0$ limits of $f^c_{\alpha\beta}(q)$ are all unity, in the partially arrested glass, a finite value less than unity is approached on the resolution of the numerical q-grid used in the calculation, for $f^c_{\rm bb}(q)$ (cf. open diamonds in Fig. 16).

As discussed above, within SCGLE the propagator matrix $\mathbf{\Psi}(q)$ appears as a natural quantity. In the partially arrested glass, the elements $\Psi_{\alpha s}(q)$ are strictly zero in SCGLE, and only at the localization transition, they rise continuously from zero to finite values. This is exemplified in Fig. 16. Within MCT, the $\Psi_{\alpha\beta}(q)$ are strictly nonvanishing, as a consequence of the (strict) positive definiteness of both $\boldsymbol{F}(q)$ and $\boldsymbol{S}(q)$. However, as shown in Fig. 16, the corresponding values $\Psi_{\alpha s}(q)$ in the partially arrested glass are *nearly* zero even within MCT. One can interpret either the SCLGE prediction, $\Psi_{\alpha s}(q) = 0$, as an approximation to small but nonzero values, or the MCT prediction, $\Psi_{\alpha s}(q) \approx 0$, as an approximation of an exact zero.

VI. CONCLUSION

We have presented and discussed asymptotic solutions for the dynamics close to conditions of dynamical arrest for two microscopic theories of the glass transition, the mode-coupling theory (MCT) and the self-consistent generalized Langevin equation theory (SCGLE). Both approaches share a very similar mathematical structure that is governed by that of a generalized Langevin equation, i.e., an integro-differential equation governed by an increasingly slowly decaying and dominant memory kernel for the density-correlation functions. Hence, the solutions of such equations are broadly similar. This notion of similarity is rendered mathematically rigorous by recognizing that the β-scaling analysis describing the asymptotic decay of the correlation functions close to the glass transition, first developed by Götze for MCT, applies to both formalisms. The appearance of asymptotic power-law decay in time is thus a robust feature shared by both theories. This extends also, broadly speaking, to further theoretical approaches such as a mode-coupling-like theory based on generalized hydrodynamics [19]. This renders them "universal" in a certain, mathematically well-defined, sense.

The most notable differences arise in the way the tagged-particle dynamics is treated. MCT focuses on the collective density correlation functions and treats the tagged-particle problem as separate, motivated by an argument that in the thermodynamic limit the effect of a single particle onto the dynamics of N others vanishes in a certain sense. SCGLE on the other hand incorporates a coupling to both collective and tagged-particle dynamics in the memory kernel of both the collective and the tagged-particle density correlations, arguing in effect that the collective friction can be thought of a combination of single-particle friction contributions.

In most cases, where the tagged-particle dynamics is closely coupled to that of the collective density fluctuations, the differences between the predictions of the two theories are consequently minor. Notably this is the case for (nearly) monodisperse HSSs, and we expect a similar conclusion to hold for many standard glass-forming systems whose interactions are dominated by strongly repulsive interactions on a typical nearest-neighbor distance (such as soft spheres or Lennard-Jones systems). The main relevant distinction between the theories in this case is the treatment of long-wavelength fluctuations, where SCGLE effectively treats the amorphous solid as infinitely rigid to first approximation. This approximation affects the calculation of hydrodynamic transport coefficients, for which MCT is expected to be the more adequate theory.

Qualitatively different descriptions emerge when one considers partially arrested glasses, i.e., the case where the self-dynamics (of at least one species) decouples from the collective slowing down. A simple example is given by the generalized Gaussian core model (GCM4), where MCT predicts the appearance of a partially arrested glass when the thermal energy is comparable or larger than the energy scale of the penetrable-core repulsion. Here, the tagged-particle motion remains ergodic at the glass transition of the collective density fluctuations and shows localization only at a higher density. Qualitatively, this scenario is in agreement with the observed appearance of a cluster-glass phase in the GCM4.

While within MCT, the peculiarities of the tagged-particle motion are not evidently incorporated into the arrest dynamics of collective density fluctuations, numerically, the delocalization of small particles in a size-disparate binary mixture leaves an imprint on the collective arrest even for the MCT predictions. In this sense, even in the treatment of partially arrested glass states, SCGLE and MCT can be seen as close approximations to each other. There it remains to be verified through experiment and simulation which description is more accurate. A recent comparison of SCGLE to both experiment and simulation of various paths to dynamical arrest in size-disparate hard-sphere mixtures has been performed as a first step in this direction [28].

The similarity of description extends from the simple liquids discussed here to more complex interactions, for example, to particles with relevant orientational degrees of freedom. A possible treatment is by a spherical-harmonics representation of the angular dependence of density fluctuations, and this route has been used in MCT [62–65] as well as in SCGLE [66]. Again, many qualitative features of the theories are in broad agreement. Also in these systems, partially arrested glasses can be found both within MCT and SCGLE, for particles whose asphericity is small enough so that certain spherical-harmonics modes of density fluctuations can decouple from the translational ones [67]. It will be interesting to test the predictions of both theories in these cases, as they represent partially arrested glasses irrespective of the collective or tagged-particle nature of the density fluctuation.

However, in the treatment of transport coefficients (such as tagged-particle diffusion and interdiffusion) the theories differ qualitatively. The interdiffusion coefficient in a binary mixture describes the collective transport mechanism

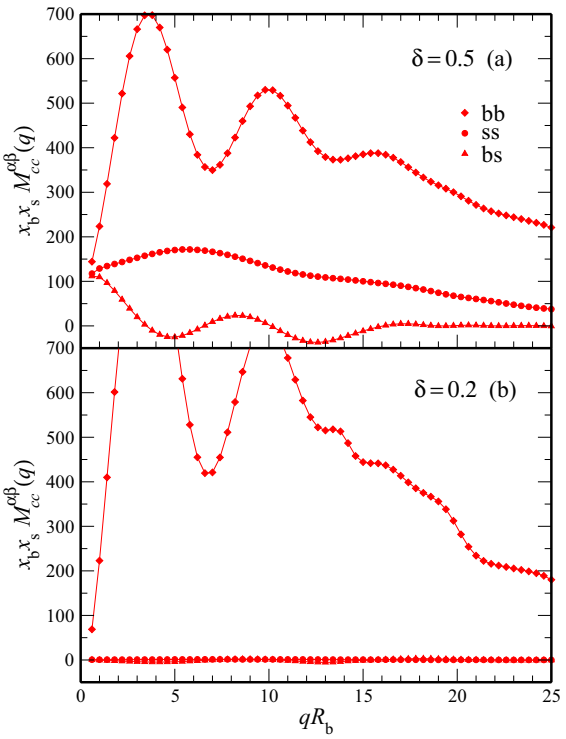

FIG. 17. Long-time limits $\lim_{t\to\infty} q^2 M_{cc}^{\alpha\beta}(q,t)$ related to the interdiffusion coefficient in a binary mixture, as obtained from MCT through the individual components of the memory kernels $q^2 m_{\alpha\beta}(q,t)$ (different symbols as labeled); see text for details. (a) Fully arrested glass ($\delta = 0.5$ and $\hat{x} = 0.2$); (b) partially arrested glass ($\delta = 0.2$ and $\hat{x} = 0.002$). The values for $q \to 0$ approach a species-independent value.

that equalizes concentration fluctuations. It can be derived on the basis of a Mori-Zwanzig equation for the concentration fluctuations $x_s\delta\varrho_b - x_b\delta\varrho_s$ in the limit $q\to 0$, and its inverse is proportional to the time integral of the corresponding memory kernel $M_{cc}(t)$ [68]. Within MCT, this memory kernel is related to the $q \to 0$ limits of the partial-current memory kernels $m_{\alpha\beta}(q,t)$ appearing in Eq. (8a) by $x_b x_s M_{cc}(t) = \hat{m}_{bb}(t)/x_s = \hat{m}_{ss}(t)/x_b = -\hat{m}_{bs}(t)/\sqrt{x_b x_s}$, where $\hat{m}_{\alpha\beta}(t) = \lim_{q\to 0} q^2 m_{\alpha\beta}(q,t)$. This symmetry in the species labels reflects the fact that in a binary mixture, a single interdiffusion coefficient exists, since concentration fluctuations of one species are linked to that of the other by the number conservation law. The SCGLE memory kernel, Eq. (7), does not have this form, and therefore it is not obvious how to extract interdiffusion coefficients from the present SCGLE.

In the (fully arrested) glass, the memory kernel $M_{cc}(t)$ of MCT approaches a finite long-time limit, and thus the interdiffusion coefficient vanishes since the time integral over $M_{cc}(t)$ diverges. It remains open how accurate this description is in partially arrested glasses, i.e., whether interdiffusion remains effective if one of the two species remains able to undergo long-range motion. Within MCT, this is only reflected through the tagged-particle memory kernels and does not explicitly appear in the equation to determine the interdiffusion coefficient. However, again, numerically the values obtained for $\lim_{t\to\infty} M_{cc}(t)$ in the partially arrested glass are close to zero. This is demonstrated in Fig. 17: we show $\lim_{t\to\infty} x_b x_s M_{cc}^{\alpha\beta}(q,t) = \lim_{t\to\infty} q^2 \hat{m}_{\alpha\beta}(q,t)/\sqrt{x_{\bar{\alpha}} x_{\bar{\beta}}}$ (where $\bar{\alpha}$ denotes the species not labeled by α) for the two exemplary glassy states discussed in Figs. 15 (left, $\hat{x} = 0.2$ for $\delta = 0.5$, a fully arrested glass) and 16 (left, $\hat{x} = 0.002$ for $\delta = 0.2$, a partially arrested glass). One recognizes in Fig. 17 that the long-time limit of $M_{cc}(q,t)$ in the fully arrested glass (for $\delta = 0.5$) approaches a finite constant as $q \to 0$, and this indicates that interdiffusion has ceased. A zero value in this limit signals finite interdiffusion, and one notes that the value obtained in the partially arrested glass ($\delta = 0.2$) is indeed close to zero.

While MCT can be regarded as more microscopically accurate, the SCGLE approach has practical advantages that it owes to its comparable simplicity. Notably it is more easily extended to nonequilibrium situations that involve aging subsequent to a temperature or density quench; the resulting theory is referred to as NE-SCGLE [69]. In the MCT framework, the rigorous extension to aging has been attempted [70], but the resulting theory is complicated to handle and has not yet yielded specific quantitative results beyond a schematic-model level [71]. One reason for the structural complexity of that nonequilibrium MCT is the need to treat both correlation and response functions as separate objects (in the absence of a fluctuation-dissipation theorem far from equilibrium) and on equal footing. NE-SCLGE allowed progress to be made under the assumption that quenches allow the static structure of the system to evolve adiabatically. The predicted scenario compares favorably to computer simulations of aging HSSs after a density quench [37] and with experimental results for dynamically arrested spinodal decomposition in systems with short-range attraction [72].

The asymptotic analysis that we presented here for SCGLE should in principle help to establish rigorous predictions also for aging systems. For example, the waiting-time dependent relaxation time of density correlation functions is found to follow a power law empirically [37,73]; it is a promising route to establish such power laws precisely as asymptotic laws in the spirit of the β-scaling analysis.

ACKNOWLEDGMENTS

We thank M. Fuchs for helpful discussions. L.F.E.A. acknowledges funding from the German Academic Exchange Service (DAAD) through the DLR-DAAD program under Grant No. 212.

[1] P. N. Pusey, in *Liquids, Freezing and Glass Transition*, edited by J. P. Hansen, D. Levesque, and J. Zinn-Justin (North-Holland, Amsterdam, 1991), pp. 765–942.

[2] L. Cipelletti and L. Ramos, J. Phys.: Condens. Matter **17**, R253 (2005).

[3] K. N. Pham, A. M. Puertas, J. Bergenholtz, S. U. Egelhaaf, A. Moussaïd, P. N. Pusey, A. B. Schofield, M. E. Cates, M. Fuchs, and W. C. K. Poon, Science **296**, 104 (2002).

[4] E. Zaccarelli and W. C. K. Poon, Proc. Natl. Acad. Sci. USA **106**, 15203 (2009).

[5] A. Meyer, J. Wuttke, W. Petry, O. G. Randl, and H. Schober, Phys. Rev. Lett. **80**, 4454 (1998).
[6] A. Meyer, Phys. Rev. B **66**, 134205 (2002).
[7] E. H. Zhou, X. Trepat, C. Y. Park, G. Lenormand, M. N. Oliver, S. M. Mijailovich, C. Hardin, D. A. Weitz, J. P. Butler, and J. J. Fredberg, Proc. Natl. Acad. Sci. USA **106**, 10632 (2009).
[8] T. E. Angelini, E. Hannezo, X. Trepat, M. Marquez, J. J. Fredberg, and D. A. Weitz, Proc. Natl. Acad. Sci. USA **108**, 4714 (2011).
[9] O. Lieleg, J. Kayser, G. Brambilla, L. Cipelletti, and A. R. Bausch, Nat. Mater. **10**, 236 (2011).
[10] D. Bi, X. Yang, M. C. Marchetti, and M. L. Manning, Phys. Rev. X **6**, 021011 (2016).
[11] W. Götze, *Complex Dynamics of Glass-Forming Liquids* (Oxford University Press, Oxford, 2009).
[12] U. Bengtzelius, W. Götze, and A. Sjölander, J. Phys. C **17**, 5915 (1984).
[13] E. Leutheusser, Phys. Rev. A **29**, 2765 (1984).
[14] W. Götze and L. Sjögren, Rep. Prog. Phys. **55**, 241 (1992).
[15] L. Yeomans-Reyna, H. Acuña-Campa, and M. Medina-Noyola, Phys. Rev. E **62**, 3395 (2000).
[16] L. Yeomans-Reyna, H. Acuña-Campa, F. de Jesús Guevara-Rodríguez, and M. Medina-Noyola, Phys. Rev. E **67**, 021108 (2003).
[17] M. A. Chávez-Rojo and M. Medina-Noyola, Phys. Rev. E **72**, 031107 (2005); **76**, 039902(E) (2007).
[18] R. Juárez-Maldonado and M. Medina-Noyola, Phys. Rev. E **77**, 051503 (2008).
[19] W. Götze and R. Schilling, Phys. Rev. E **91**, 042117 (2015).
[20] T. Franosch, M. Fuchs, W. Götze, M. R. Mayr, and A. P. Singh, Phys. Rev. E **55**, 7153 (1997).
[21] M. Fuchs, W. Götze, and M. R. Mayr, Phys. Rev. E **58**, 3384 (1998).
[22] T. Gleim, W. Kob, and K. Binder, Phys. Rev. Lett. **81**, 4404 (1998).
[23] G. Szamel and E. Flenner, Europhys. Lett. **67**, 779 (2004).
[24] W. Götze and L. Sjögren, J. Math. Anal. Appl. **195**, 230 (1995).
[25] T. Franosch and Th. Voigtmann, J. Stat. Phys. **109**, 237 (2002).
[26] Th. Voigtmann, Phys. Rev. E **68**, 051401 (2003).
[27] T. Sentjabrskaja, E. Zaccarelli, C. De Michele, F. Sciortino, P. Tartaglia, T. Voigtmann, S. U. Egelhaaf, and M. Laurati, Nat. Commun. **7**, 11133 (2016).
[28] E. Lázaro-Lázaro, J. A. Perera-Burgos, P. Laermann, T. Sentjabrskaja, G. Pérez-Ángel, M. Laurati, S. U. Egelhaaf, M. Medina-Noyola, T. Voigtmann, R. Castaneda-Priego, and L. F. Elizondo-Aguilera, Phys. Rev. E **99**, 042603 (2019).
[29] J. Horbach, W. Kob, and K. Binder, Phys. Rev. Lett. **88**, 125502 (2002).
[30] Th. Voigtmann and J. Horbach, Europhys. Lett. **74**, 459 (2006).
[31] G. Szamel and H. Löwen, Phys. Rev. A **44**, 8215 (1991).
[32] E. Lázaro-Lázaro, P. Mendoza-Méndez, L. F. Elizondo-Aguilera, J. A. Perera-Burgos, P. E. Ramírez-González, G. Pérez-Angel, R. Castañeda-Priego, and M. Medina-Noyola, J. Chem. Phys. **146**, 184506 (2017).
[33] J.-P. Hansen and I. R. McDonald, *Theory of Simple Liquids*, 3rd ed. (Academic Press, London, 2006).
[34] M. Medina-Noyola, Faraday Discuss. Chem. Soc. **83**, 21 (1987).
[35] M. Medina-Noyola and J. L. del Rio-Correa, Phys. A: Stat. Mech. Applic. **146**, 483 (1987).
[36] M. Hernández-Contreras, M. Medina-Noyola, and A. Vizcarra-Rendón, Physica A (Amsterdam) **234**, 271 (1996).
[37] P. Mendoza-Méndez, E. Lázaro-Lázaro, L. E. Sánchez-Díaz, P. E. Ramírez-González, G. Pérez-Ángel, and M. Medina-Noyola, Phys. Rev. E **96**, 022608 (2017).
[38] W. Götze and Th. Voigtmann, Phys. Rev. E **67**, 021502 (2003).
[39] W. Götze and M. R. Mayr, Phys. Rev. E **61**, 587 (2000).
[40] M. Fuchs and T. Voigtmann, Philos. Mag. B **79**, 1799 (1999).
[41] S. Mandal, T. Franosch, and Th. Voigtmann, Soft Matter **14**, 9153 (2018).
[42] L. Yeomans-Reyna, M. A. Chávez-Rojo, P. E. Ramírez-González, R. Juárez-Maldonado, M. Chávez-Páez, and M. Medina-Noyola, Phys. Rev. E **76**, 041504 (2007).
[43] W. van Megen and S. M. Underwood, Phys. Rev. Lett. **70**, 2766 (1993).
[44] W. van Megen and H. J. Schöpe, arXiv:1810.03778 (2018).
[45] M. Fuchs, J. Non-Cryst. Solids **172**, 241 (1994).
[46] A. J. Moreno and C. N. Likos, Phys. Rev. Lett. **99**, 107801 (2007).
[47] C. N. Likos, B. M. Mladek, A. J. Moreno, D. Gottwald, and G. Kahl, Comput. Phys. Commun. **179**, 71 (2008).
[48] D. Coslovich, L. Strauss, and G. Kahl, Soft Matter **7**, 2127 (2011).
[49] D. Coslovich, M. Bernabei, and A. J. Moreno, J. Chem. Phys. **137**, 184904 (2012).
[50] A. Ikeda and K. Miyazaki, Phys. Rev. Lett. **106**, 015701 (2011).
[51] A. Ikeda and K. Miyazaki, J. Chem. Phys. **135**, 054901 (2011).
[52] V. Krakoviack, Phys. Rev. Lett. **94**, 065703 (2005); Phys. Rev. E **75**, 031503 (2007).
[53] V. Krakoviack, Phys. Rev. E **79**, 061501 (2009).
[54] S. K. Schnyder, F. Höfling, T. Franosch, and T. Voigtmann, J. Phys.: Condens. Matter **23**, 234121 (2011).
[55] R. Miyazaki, T. Kawasaki, and K. Miyazaki, J. Chem. Phys. **150**, 074503 (2019).
[56] T. Voigtmann, Europhys. Lett. **96**, 36006 (2011).
[57] G. Foffi, W. Götze, F. Sciortino, P. Tartaglia, and T. Voigtmann, Phys. Rev. Lett. **91**, 085701 (2003); Phys. Rev. E **69**, 011505 (2004).
[58] K. Dawson, G. Foffi, M. Fuchs, W. Götze, F. Sciortino, M. Sperl, P. Tartaglia, T. Voigtmann, and E. Zaccarelli, Phys. Rev. E **63**, 011401 (2000).
[59] W. Götze and M. Sperl, Phys. Rev. E **66**, 011405 (2002).
[60] M. Sperl, Phys. Rev. E **68**, 031405 (2003).
[61] M. Sperl, Phys. Rev. E **69**, 011401 (2004).
[62] R. Schilling and T. Scheidsteger, Phys. Rev. E **56**, 2932 (1997).
[63] T. Franosch, M. Fuchs, W. Götze, M. R. Mayr, and A. P. Singh, Phys. Rev. E **56**, 5659 (1997).
[64] M. Letz, R. Schilling, and A. Latz, Phys. Rev. E **62**, 5173 (2000).
[65] R. Schilling, Phys. Rev. E **65**, 051206 (2002).
[66] L. F. Elizondo-Aguilera, P. F. Zubieta Rico, H. Ruiz-Estrada, and O. Alarcón-Waess, Phys. Rev. E **90**, 052301 (2014).
[67] S.-H. Chong, A. J. Moreno, F. Sciortino, and W. Kob, Phys. Rev. Lett. **94**, 215701 (2005).
[68] M. Fuchs and A. Latz, Physica A **201**, 1 (1993).

[69] P. Ramírez-González and M. Medina-Noyola, Phys. Rev. E **82**, 061503 (2010); **82**, 061504 (2010).
[70] A. Latz, J. Phys.: Condens. Matter **12**, 6353 (2000).
[71] B. Kim and A. Latz, Europhys. Lett. **53**, 660 (2001).
[72] J. M. Olais-Govea, L. López-Flores, M. Chávez-Páez, and M. Medina-Noyola, Phys. Rev. E **98**, 040601(R) (2018).
[73] L. E. Sánchez-Díaz, P. Ramírez-González, and M. Medina-Noyola, Phys. Rev. E **87**, 052306 (2013).